Minerals Engineering 159 (2020) 106617

Contents lists available at ScienceDirect

Minerals Engineering

journal homepage: www.elsevier.com/locate/mineng

Key process mineralogy parameters for rare earth fluorcarbonate-bearing carbonatite deposits: The example of Songwe Hill, Malawi

Safaa Al-Ali[a,b,*], Frances Wall[a], Robert Fitzpatrick[a], Sam Broom-Fendley[a], Gavyn Rollinson[a], Aoife E. Brady[c], Jonathan R. Pickles[a], Adam Williams[a], Will Dawes[d]

[a] Camborne School of Mines, University of Exeter, Penryn Campus, Penryn, Cornwall TR10 9FE, United Kingdom
[b] Department of Geology, College of Science, University of Basrah, Basrah 61004, Iraq
[c] CRAG, O'Brien Centre for Science (East), University College Dublin, Belfield, Dublin 4, Ireland
[d] Mkango Resources Ltd., 550 Burrard Street, Suite 2900, Vancouver, BC V6C 0A3, Canada

ARTICLE INFO

Keywords:
Process mineralogy
Rare earth elements
Synchysite-(Ce)
Apatite
Carbonatite
Songwe Hill

ABSTRACT

Rare earth element (REE)-bearing carbonatite deposits commonly contain a wide range of different REE- and REE-bearing minerals associated with various gangue matrices. In order to select the most-suitable mineral processing technique for these deposits, it is essential to identify and quantify the minerals of interest, including their liberation, associations and grain size distribution, along with whole rock compositions. These data are also vital for ore feed optimisation and metallurgical troubleshooting during and after designing a mineral processing flowsheet. This paper summarises the key mineralogical parameters needed before conducting metallurgical beneficiation tests, using the Songwe Hill carbonatite deposit as an example. This REE ore deposit consists of poorly-liberated synchysite-(Ce), which hosts the light rare earth elements including Nd plus some heavy rare earths and well-liberated apatite, which hosts 50% of Gd, 63% of Dy and 71% of Y (heavy rare earth elements) in the deposit. For all REE heavier than Gd, apatite is the most important REE host, however, for the two REE where data are available in both synchysite-(Ce) and apatite (Dy and Y), synchysite-(Ce) still accommodates > 25% of the whole-rock HREE content. Both of these ore minerals are associated with ankerite, calcite, and to a lesser extent with iron oxides/carbonates, K-feldspar, strontianite and baryte. According to the quantitative mineralogical data, the possibility of using gravity separation, magnetic separation, froth flotation and leaching to process Songwe Hill carbonatite ore is discussed and a potential beneficiation flowsheet is presented.

1. Introduction

Characterising mineralogical textures in an ore body is a powerful and integrated tool for designing processing routes and improving separation performance (Gottlieb et al., 2000; Lotter et al., 2002; Evans et al., 2011). A successful separation process mainly depends on exploiting differences in physical and chemical properties (such as specific gravity, magnetic and electrostatic response and surface chemistry) between particles containing ore and gangue minerals. Identification and quantification of the key mineralogical parameters, such as mineral identity and abundance, liberation, association, and grain size distribution also play a significant role in predicting the possible flowsheet options for processing an ore deposit. These are vital for metallurgical troubleshooting and data interpretation during and after the design of a mineral processing flowsheet.

Carbonatite deposits are the largest and highest grade sources for the REE (Jackson and Christiansen, 1993; Wall, 2014). These rocks vary in composition from calciocarbonatite to ferrocarbonatite (Woolley and Kempe, 1989) and can host multiple REE minerals such as the fluorcarbonates (bastnäsite, parisite, synchysite), monazite, ancylite and, less commonly, xenotime and allanite as well as REE-bearing minerals such as apatite, which is common as a rock-forming mineral. These REE minerals are associated with a wide range of gangue phases, such as calcite, dolomite, ankerite, forsterite, aegirine, phlogopite, biotite, magnetite and other iron oxides. Due to the mineralogical variety and complexity of carbonatites, it is essential to identify the carbonatite type and the minerals that host REE. With this knowledge, it is possible to determine key physical, chemical and mineralogical characteristics before considering any mineral processing route. Owing to the complexity of mineral processing in carbonatites, mineralogy is more important than grade at the early stages of exploration.

The rare earth minerals commercially extracted from carbonatites

* Corresponding author at: Camborne School of Mines, University of Exeter, Penryn Campus, Penryn, Cornwall TR10 9FE, United Kingdom.
E-mail address: safaa.alali@outlook.com (S. Al-Ali).

https://doi.org/10.1016/j.mineng.2020.106617
Received 29 April 2020; Received in revised form 26 August 2020; Accepted 1 September 2020

Table 1
Examples of REE ore deposits that contain synchysite.

REE deposit	Lithology	REE minerals	Reserve and grade	Reference
Springer Lavergne, ON, Canada	Carbonatite	Synchysite-(Ce)	16.9 Mt at ~1.16 wt% TREO	Mariano and Mariano (2012), Daigle (2012)
Adiounedj, Mali	Carbonatite	Synchysite-(Ce)	No data	Wall and Mariano (1996), Verplanck et al. (2015)
Lugiin Gol, Mongolia	Nepheline syenite	Synchysite-(Ce)	0.023 Mt at 3.2% TREO	Haumdas et al. (1995), Krishnamurthy and Gupta (2016)
Kutessay, Kyrgyzstan	Granite	Monazite, monazite, xenotime, bastnäsite-(Y), parisite-(Y) and synchysite-(Y)	16.28 Mt at 0.264% TREO	Chakhmouradian and Wall (2012), Hyland and Ulrich (2014), Stans Energy Corp.
Barra do Itapirapuã, Brazil	Carbonatite	Parisite, synchysite and rare bastnäsite	No data	Ruberti et al. (2008), Chakhmouradian and Wall (2012)
Gatineau, Quebec, Canada	Carbonatite	Parisite-(Ce), synchysite-(Ce) and monazite	No data	Hogarth et al. (1985)
Miaoya, China	Carbonatite	Bastnäsite, synchysite and monazite	1.72%	Kynicky et al. (2012)
Huanglongpu, China	Carbonatite	Bastnäsite, synchysite, monazite and xenotime	No data	Kynicky et al. (2012)
Huayangchuan, China	Carbonatite	Bastnäsite, synchysite, xenotime and allanite	No data	Kynicky et al. (2012)
Mt. Prindle, AK, USA	Hydrothermal mineralisation in syenite	Britholite, parisite and synchysite	No data	Mariano and Mariano (2012)
Rock Canyon Creek, BC, Canada	Carbonatite	Monazite, synchysite, bastnäsite and gorceixite	No data	Mariano and Mariano (2012)
Mountain Pass, CA, USA	Calcite and dolomite carbonatite	Bastnäsite, parisite and synchysite	20–47 Mt at 8.9% TREO	Wall and Mariano (1996), Krishnamurthy and Gupta (2016)
Bear Lodge, WY, USA	Carbonatite	Bastnäsite, parisite, synchysite, ancylite, monazite and cerianite	34.3 Mt at 3.05% TREO	Dahlberg et al. (2014)
Nechalacho (Thor Lake), Canada	Peralkaline syenite	Allanite, monazite, bastnäsite, synchysite, HREE in fergusonite, zircon	4.3 Mt REO 107.59 Mt at 1.26–1.48% REO	Avalon Rare Metals (2013)
Khaldzan-Buregtey, Western Mongolia	Peralkaline granite, gabbro, basalt, pantellerite dikes, syenite	Fergusonite, allanite, bastnäsite, synchysite, britholite, monazite and chevkinite	> 1.2 Mt at 0.3% TREE	Krishnamurthy and Gupta (2016)
Wigu Hill, Tanzania	Weathered dolomitic carbonatite	Bastnäsite, monazite, goyazite, synchysite and parisite	As much as 20% TREO	Krishnamurthy and Gupta (2016)
Wet Mountains, CO, USA	Magmatic Alkaline rocks, arbonatite Dikes thorite, xenotime, baryte, hematite, quartz	Apatite, bastnäsite, synchysite, xenotime and monazite	13.96 Mt at 1.0% TREO	Krishnamurthy and Gupta (2016)
Khibina (Khibiny) Kola Peninsula, Russia	Foyaite, nepheline syenite, ijolite, rischorrite, urtite, pegmatites, carbonatite	Apatite, eudialyte, burbankite and ancylite, synchysite, parisite, carbocernaite, cordylite, astrophyllite, loparite, mosandrite, lovchorrite and rinkite	9 Mt TREO	Nivin et al. (2005), Krishnamurthy and Gupta (2016)
Ngualla Hill, Tanzania	Carbonatite	Bastnäsite and monazite	214.4 Mt at 2.15% TREO	Peak Resources Ltd.

are bastnäsite-(Ce), the Ca-free end-member of the REE fluorcarbonate group, and monazite-(Ce). Xenotime has also been processed from other REE deposit types (Jordens et al., 2013; Krishnamurthy and Gupta, 2016). Bastnäsite deposits (e.g. Mountain Pass and Bayan Obo) usually contain minor amounts of the other REE fluorcarbonates. One of these, synchysite-(Ce), the Ca-rich end-member REE fluorcarbonate, is one of the most-commonly occurring REE minerals and the second most reported mineral of the REE fluorcarbonate group (Wang et al., 1994). To demonstrate this, we have compiled a list of deposits which contain synchysite as a valuable mineral (Table 1). Despite the abundance of synchysite-(Ce) as a REE mineral, it is not currently commercially extracted as a major ore mineral. Research thus far has focussed on understanding the potential processing options for synchysite-(Ce), such as roasting to improve acid solubility (Burmaa et al., 2007), magnetic separation (Al-Ali et al., 2019) and flotation (Owens et al., 2018, 2019). However, there have been few studies that integrate geological and mineralogical observations of a REE-rich carbonatite to predict how synchysite-(Ce), and other ore minerals, behave during mineral processing (e.g., Schulz et al., 2019; Van Rythoven et al., 2020; Jiao et al., 2020). In this contribution we undertake such a study, using the Songwe Hill carbonatite as an example, in order to evaluate and discuss the fundamental mineralogical parameters that need considering for the design of an appropriate beneficiation flowsheet for synchysite-rich deposits.

2. A case study – The Songwe Hill rare earth project

The Songwe Hill carbonatite deposit, Malawi, is an advanced rare earth project, licensed to Mkango Resources Ltd., and is the case study of this article. It is interpreted as a circular volcanic vent approximately 800 m in diameter and comprises a multi-phase intrusion composed of carbonatite, fenite and breccia (Broom-Fendley et al., 2017a; Witley et al., 2020). REE mineralisation is disseminated throughout the deposit. In the field, the rocks are locally brecciated and cross-cut by veins, some of which are REE-rich, while others are barren (Broom-Fendley et al., 2017a). However, at the wider scale relevant to industrial mining (~10 m blocks), the deposit is relatively homogeneous in terms of its REE mineralogy and grade. The principal REE-bearing minerals in this ore deposit are apatite and synchysite-(Ce).

Apatite is anomalously enriched in the heavy rare earth elements (HREE: Eu–Lu + Y), compared to apatite in most carbonatite deposits (Broom-Fendley et al., 2016, 2017b), while synchysite-(Ce) is light rare earth element (LREE: La–Sm) rich. In this article, we focus on apatite and synchysite-(Ce) as “valuable minerals” for their content of REE, although minor florencite-(Ce), parisite-(Ce) and trace bastnäsite and monazite do also occur.

3. Materials and analytical methods

Preparation and analysis of whole-rock powders was carried out by Intertek-Genalysis Laboratory Services Pty Ltd. in Johannesburg, South Africa, and Perth, Australia. All other analytical work was carried out at Camborne School of Mines, University of Exeter.

3.1. Materials

In total, fifteen carbonatite rock samples of different size fractions were analysed for their bulk chemical and mineralogical composition, and for particle size distribution. These samples consist of eight crushed drill core samples representing eight drill holes from Songwe Hill with a P_{100} of 1700 μm, two composite samples with P_{80} of 53 μm and 38 μm, and five size-by-size fractions of > 40 μm, 30–40 μm, 20–30 μm, 10–20 μm, and < 10 μm (Fig. 1). The location and lithology of the drill cores used in this study are shown in Fig. 2.

The crushed samples with P_{100} of 1700 μm were treated separately by splitting each whole sample (about 4 kg) into small fractions to produce three representative subsamples of approximately 30 g each using a riffle splitter. One of the subsamples was used to represent the individual crushed drill core, whereas the other subsamples were used to make two composite samples (Fig. 1). The composite samples were made by combining the subsamples from individual drill cores and then using a rod mill to produce 53 μm and 38 μm fractions. Size-by-size fractions were obtained from the remaining portion of the 53 μm ground sample using a Warman Cyclosizer, producing fractions between approximately > 40 μm and < 10 μm. All the size fractions were filtered, dried and riffled into representative subsamples. Each size fraction of the riffled subsamples was further reduced by a rotary microriffler to about 1 g, as a final representative subsample. These fractions were then prepared as polished blocks for mineralogical analyses.

3.2. Whole rock chemistry

Crushed drill core samples were analysed for REE, Mg, Al, Si, P, S, K, Ca, Mn, Fe, Sr, Zr, Nb, Th and U contents. The samples were milled and pulverised to 80% passing size P_{80} of 75 μm. Milled powders were digested as a sodium peroxide fusion to ensure complete dissolution. After digestion, the sample was diluted and analysed using inductively coupled plasma optical emission spectrometry (ICP-OES) for the major elements and inductively coupled plasma mass spectrometry (ICP-MS) for the REE and other trace elements (Witley et al., 2020). Internal quality assurance and quality control procedures included the insertion of duplicate samples, blanks and certified reference materials (AMIS0185, GRE-04). The results indicated no contamination nor analytical issues (Witley et al., 2020).

3.3. X-ray diffraction

Samples were disaggregated with an agate mortar and pestle and then analysed using a Siemens D5000 X-ray diffractometer. Analyses were carried out using a Cu Kα source operated with a tube voltage of 40 kV and current of 30 mA. The profile produced by the scan was interpreted using the JCPDS PDF-2 (2004) database and Bruker EVA software V.10.0.1.0.

3.4. SEM and electron probe microanalysis

Initial mineral identification was first undertaken by SEM-EDS using a JEOL JSM-5400LV Low Vacuum SEM, equipped with Oxford Instruments EDS system. Following this, mineral compositions were determined using a JEOL JXA-8200 EPMA, operated with a 15 kV accelerating voltage, 20 nA beam current, and 5 μm beam diameter. The peak counting times were 10 s for La and Ce; 20 s for Pr, Nd, Sm, Eu, Gd, Dy, Er, Y, Th, and U; and 30 s for Ca, P, and F. The REE were calibrated using synthetic silicate glasses from the Edinburgh Ion Probe Facility, while the other elements were calibrated against a combination of natural and synthetic minerals and metals. A manual correction was applied to the REE data to account for X-ray peak overlaps, such as those of Ce on Sm and Gd.

3.5. Automated mineralogy by QEMSCAN®

Automated mineralogical analyses were carried out using QEMSCAN® (*Quantitative Evaluation of Minerals by Scanning Electron Microscopy*) 4300 system. The instrument was operated using a 25 kV, 5 nA electron beam and an X-ray collection rate of 1000 counts (Rollinson et al., 2011). A 10 μm spatial resolution was set for the crushed drill core samples, while 1 μm spatial resolution was set for the composite samples and the size-by-size fractions. QEMSCAN® operation followed quality control procedures developed in-house for sample preparation, instrument calibration, operation and data processing (Rollinson et al., 2011).

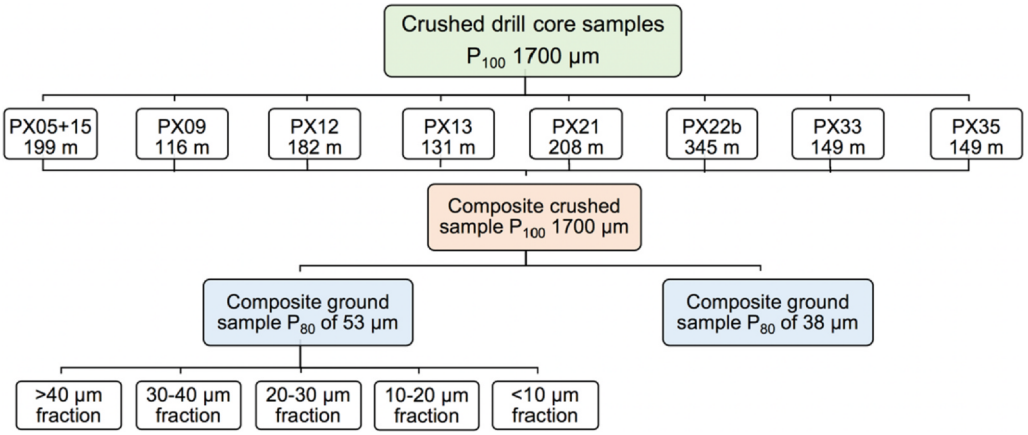

Fig. 1. Summary of the samples used in this work. "PX05–35" are drill hole identifiers.

3.5.1. *Differentiation of individual REE fluorcarbonates minerals*

Using automated mineralogical techniques to determine different REE minerals is challenging (e.g., Sindern and Meyer, 2016; Schulz et al., 2019; Van Rythoven et al., 2020; Jiao et al., 2020). Therefore, a species identification protocol (SIP) was developed using internal reference mineral standards, validated by SEM-EDS and EPMA, to differentiate chemically-similar REE minerals such as synchysite-(Ce) and parisite-(Ce), which frequently occur as syntaxial intergrowths (Fig. 3A). Development of the SIP was carried out iteratively using Ca X-ray count rate levels of 85, 88, and 90, with the best result obtained using a Ca level of 88 (Fig. 3B). Owing to the common occurrence of intergrowths of apatite and florencite at scales smaller than the 10 µm resolution, an "apatite/florencite" term is used herein for this mixed phase.

3.6. *Particle size analysis and classification*

A Malvern Mastersizer MAF500 laser-sizer was used to determine the particle size distribution of the composite samples with P_{80} of 53 µm and 38 µm. The ground sample was suspended in a beaker using a rotating impeller, from which about 5–10 mL was collected using a pipette and introduced into the Malvern Mastersizer.

The ground composite sample P_{80} of 53 µm was wet screened using a vibrating mechanical 45 µm sieve before analysing using the Mastersizer. The < 45 µm size fraction was further classified by a Warman Cyclosizer to separate particles into different size fractions. Approximately 75 g of ground sample was mixed with water and run on the Cyclosizer for 30 min at 20 °C. Each collected sample was allowed to settle before being decanted, pressure filtered, dried and weighed. The density of each size fraction was measured using a Micromeritics AccuPyc 1330 instrument. The equivalent diameter of the five cyclones

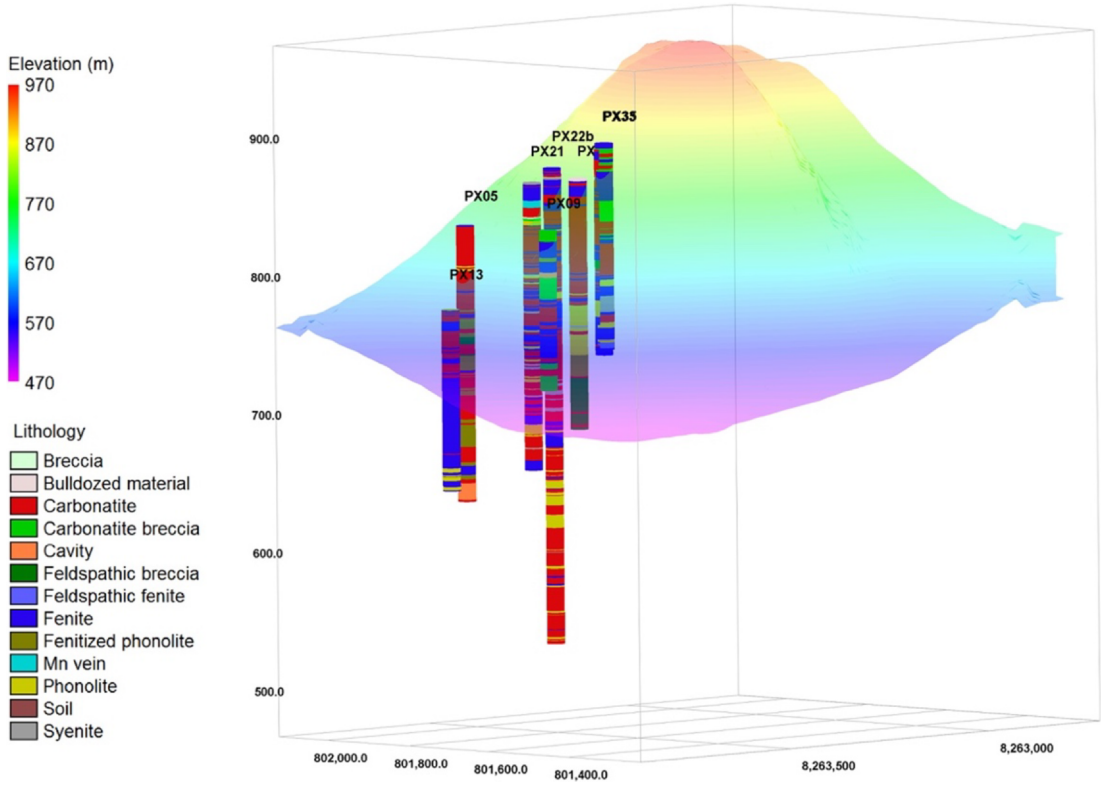

Fig. 2. A 3D model of Songwe Hill and location of the drill holes. Elevation data are from Google Earth and the lithology of the drill cores from Mkango Resources Ltd.

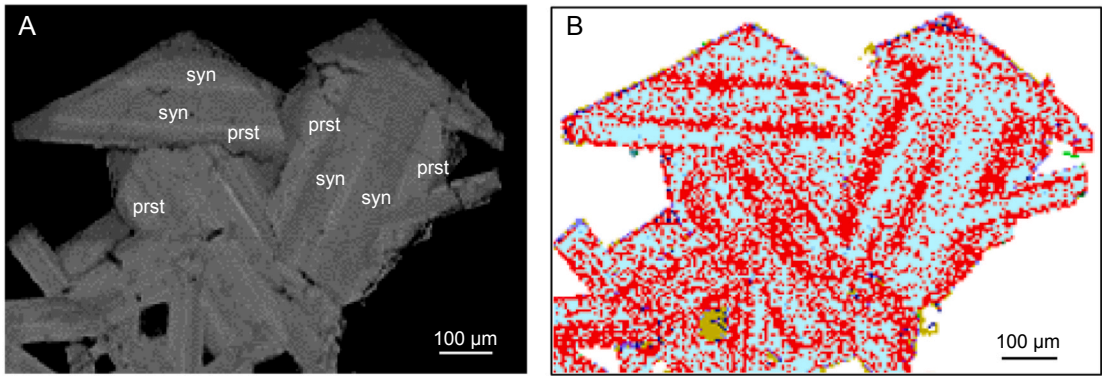

Fig. 3. (A) BSE image showing syntaxial intergrowth of synchysite-(Ce) (dark grey) and parisite-(Ce) (grey) crystals and (B) false-coloured fieldscan image showing syntaxial intergrowth of synchysite-(Ce) (light blue) and parisite-(Ce) (red) crystals as determined by automated mineralogy. (For interpretation of the references to colour in this figure legend, the reader is referred to the web version of this article.)

and the consequent down-stream size fractions were: 41 µm, 30 µm, 21 µm, 14 µm, 10 µm and < 10 µm.

4. Key process mineralogy parameters

4.1. Mineralogy

Identifying and quantifying minerals of interest, including their liberation, association, and grain size distribution, is a fundamental component of the process mineralogy. It improves understanding of the ore body and provides insight into the target minerals and optimum grind size of the feed before conducting any mineral processing testwork. It is also vital information for ore feed optimisation and metallurgical troubleshooting during and after the design of a mineral processing flowsheet (Gottlieb et al., 2000; Grammatikopoulos et al., 2013; Van Rythoven et al., 2020).

Observations from SEM images, combined with XRD and automated mineralogy data, indicate that all the drill core samples have a similar mineralogical composition, but vary slightly in their relative proportions. The main gangue minerals are calcite, ankerite and K-feldspar along with traces of strontianite, baryte, hematite, goethite and siderite (Fig. 4). Apatite, synchysite-(Ce) and florencite-(Ce) are the predominant valuable minerals.

Automated mineralogical analyses show that the carbonatite at Songwe Hill contains about 7–10 wt% apatite, synchysite-(Ce) and florencite-(Ce), as well as trace amounts of bastnäsite and monazite (Table 2; Fig. 5).

From back-scattered electron imagery, it is evident that the valuable minerals are typically fine-grained, and commonly between 5 and 50 µm in size. Between samples they vary in their proportions and crystal shapes, particularly synchysite-(Ce). In addition, they are associated with all gangue minerals, indicative of a complex ore deposit.

Apatite commonly occurs as subhedral to anhedral grains in patchy or vein-like textures, with a grain size up to 100 µm. It is mostly associated with ankerite followed by calcite and to a lesser extent with K-feldspar and Fe/Mn oxides (Fig. 6A). It also occurs as a well-liberated coarse-grained phase up to 400 µm (Fig. 6B).

Synchysite-(Ce) commonly occurs as fine to very fine anhedral to subhedral grains, < 25 µm diameter, as assemblages of fibro-radial crystals which form nest-like microstructures or individual platy (acicular cross-section) crystals (Fig. 6C). It also, to a lesser extent, occurs as granular (lath-shaped) crystals of about 150 µm (Fig. 6D). It is primarily associated with calcite and ankerite, as well as strontianite, baryte and Fe/Mn oxides. Synchysite-(Ce) crystals are mostly locked and poorly liberated.

Crystal shape and size are important parameters for processing an ore deposit as both can affect the degree of liberation. Where synchysite occurs as very thin platy (needle-like) crystals, liberation may be

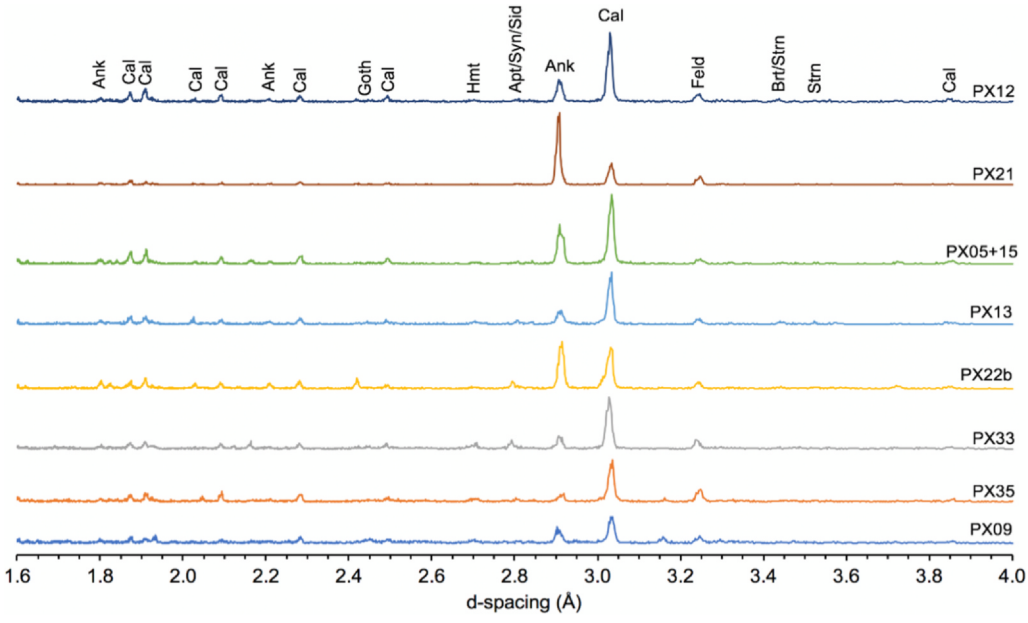

Fig. 4. Mineralogical composition of the crushed drill core carbonatite samples of Songwe Hill as determined by XRD. All peaks are normalised based on the maximum peak intensity in each XRD profile. Abbreviations: Ank: ankerite, Apt: apatite, Brt: baryte, Cal: calcite, Feld: K-feldspar, Goth: goethite, Hmt: hematite, Sid: siderite, Strn: strontianite, Syn: synchysite-(Ce).

Table 2
Quantitative modal mineralogical data (wt%) of the valuable and gangue minerals in the composite samples and the size-by-size fractions of the ground composite sample P_{80} of 53 μm determined by automated mineralogy.

Mineral group		Mineral name	Composite samples (μm)			Size-by-size fractions (μm)				
			1700	53	38	> 40	30–40	20–30	10–20	< 10
Valuable minerals	Phosphates	Apatite	3.78	5.56	5.01	4.96	4.15	3.38	3.36	4.74
		Florencite-(Ce)	0.32	0.60	0.64	0.28	0.42	0.61	0.49	0.70
		Apatite/florencite-(Ce)	0.40	0.42	0.57	0.15	0.25	0.18	0.21	0.59
		Monazite	0.01	0.01	0.02	0.01	0.02	0.01	0.01	0.01
	Carbonates	Synchysite-(Ce)/parisite-(Ce)	2.46	3.22	2.69	2.68	3.37	3.12	3.05	4.25
		Bastnäsite	0.02	0.01	0.01	0.01	0.01	0.03	0.04	0.03
Gangue minerals	Carbonates	Calcite	29.28	27.04	26.61	21.99	26.16	32.97	35.79	25.62
		Ankerite	31.05	30.34	30.69	33.96	35.20	30.46	27.09	28.72
		Dolomite	0.12	0.20	0.33	0.23	0.19	0.23	0.15	0.12
		Strontianite	1.49	1.17	1.62	1.54	2.08	1.26	1.13	0.75
	Silicates	K-feldspar	9.40	9.52	9.89	9.49	5.93	10.49	9.66	8.38
		Plagioclase	0.13	0.17	0.17	0.07	0.06	0.13	0.09	0.51
		Biotite	0.66	0.45	0.55	0.57	0.38	0.37	0.48	0.65
		Chlorite	0.39	0.63	0.75	0.28	0.24	0.21	0.31	1.61
		Kaolinite	0.02	0.01	0.01	0.01	0.01	0.01	0.01	0.01
		Quartz	0.17	0.14	0.16	0.18	0.20	0.25	0.24	0.43
		Zircon	0.01	0.03	0.10	0.01	0.03	0.03	0.06	0.03
		Other silicates	1.65	1.87	1.83	1.30	1.17	1.42	1.64	3.17
	Oxides	Fe-Ox(Mn)/CO_3 [a]	13.73	12.69	12.16	14.77	13.29	10.03	10.91	14.56
		Mn Ox/CO_3	0.19	0.34	0.47	0.28	0.23	0.24	0.32	0.53
		Rutile	0.52	0.71	1.04	0.74	0.59	0.33	0.43	0.55
		Ilmenite	0.86	0.67	0.50	1.47	0.86	0.65	0.58	0.23
		Pyrophanite	0.32	0.33	0.44	0.86	0.67	0.42	0.44	0.29
		Pyrochlore	0.38	1.18	0.34	0.97	0.48	0.34	0.40	0.14
	Sulphides	Pyrite	0.37	0.24	0.15	0.48	0.42	0.12	0.19	0.44
		Sphalerite	0.01	< 0.01	< 0.01	0.03	0.10	0.03	0.04	0.02
		Galena	0.01	< 0.01	< 0.01	0.01	0.08	0.01	0.01	0.01
	Sulphates	Baryte	1.36	0.98	2.20	1.41	1.96	1.27	1.64	1.73
		Gypsum	0.00	0.04	0.06	0.01	0.01	0.01	0.02	0.07
	Halides	Fluorite	0.87	1.03	0.88	1.08	1.39	1.37	1.18	1.05
	Mixed	Others [b]	0.01	0.09	0.08	0.19	0.05	0.05	0.04	0.08

[a] Including magnetite, jacobsite, titaniferous magnetite, siderite, hematite, goethite and limonite (Williams, 2019) and the average density of these minerals is used to convert the data into wt%.
[b] Others includes traces of any other minerals not listed above.

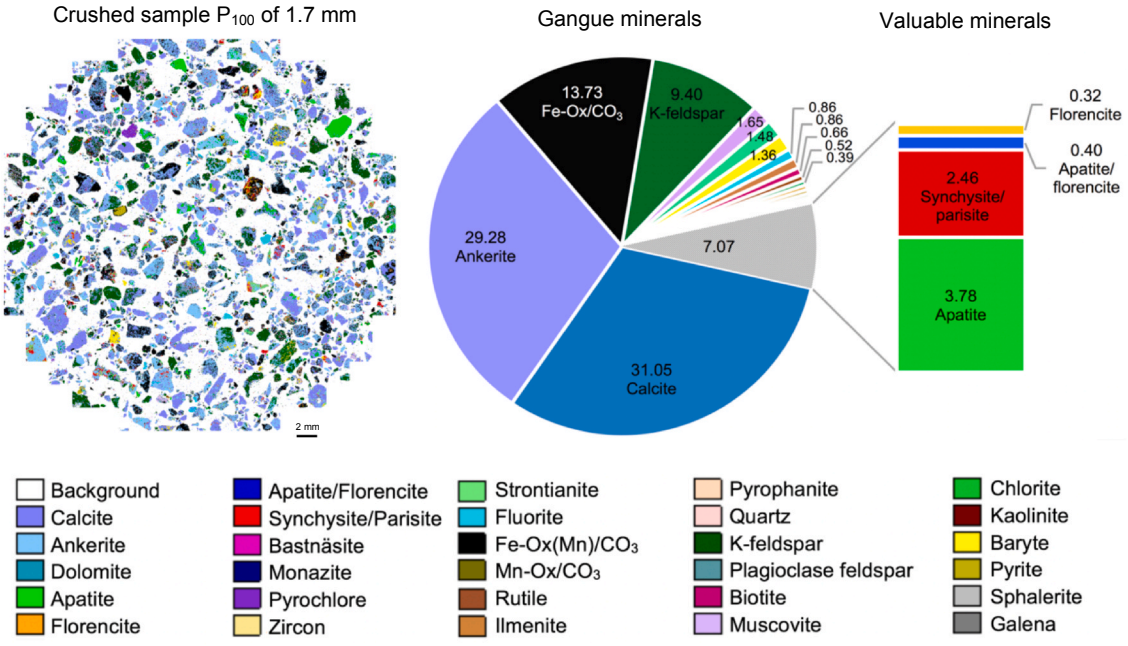

Fig. 5. A false-coloured image along with mineralogical composition data (wt%) of the valuable and gangue minerals in the composite crushed drill core sample P_{100} of 1700 μm as determined by automated mineralogy.

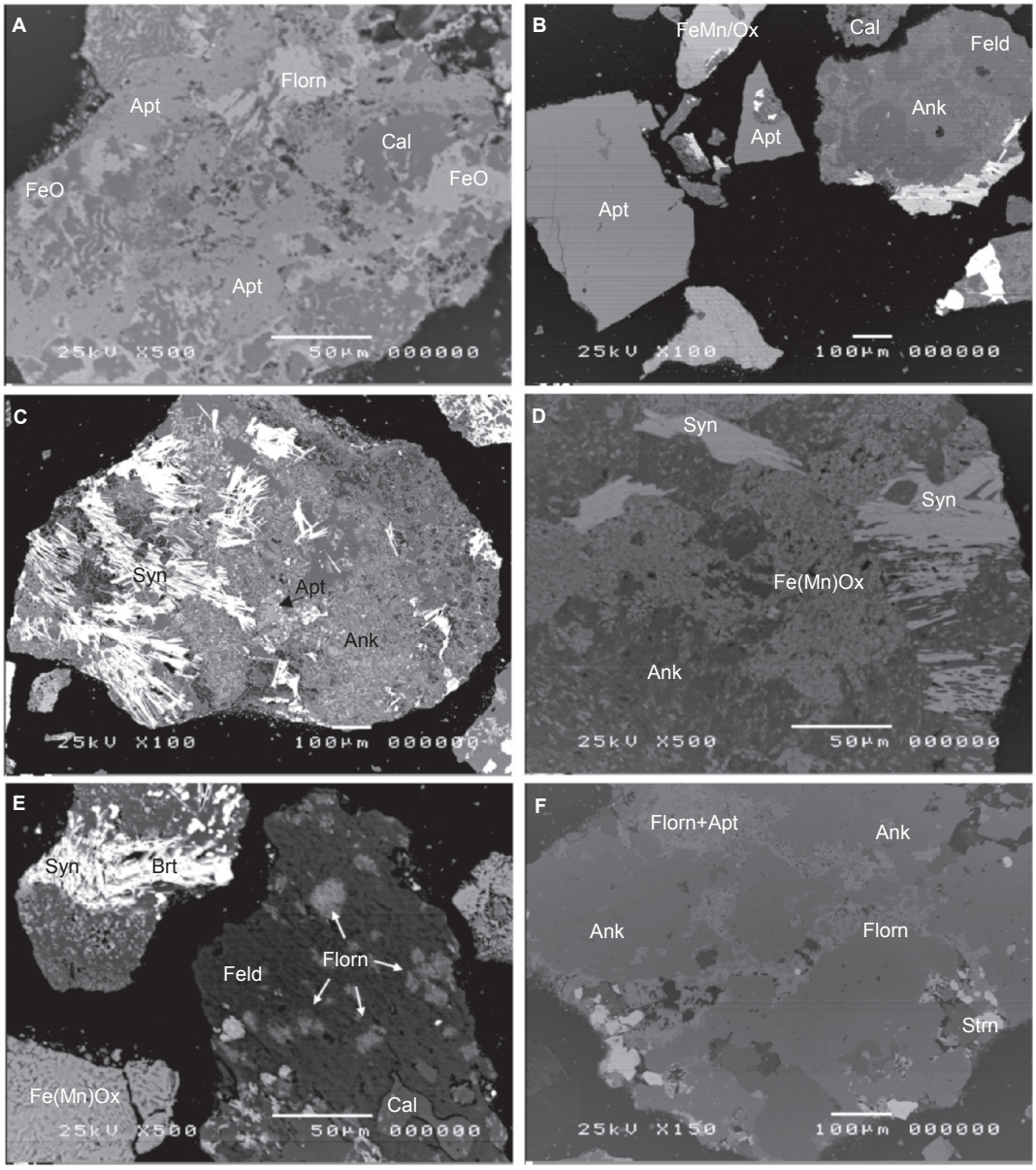

Fig. 6. Examples of apatite, synchysite-(Ce) and florencite-(Ce) crystal shapes: (A) patchy vein-like apatite associated with calcite and iron oxides/carbonates, (D) very large liberated particles of apatite, (C) assemblages of acicular crystals of synchysite-(Ce) associated with ankerite, (D) granular crystals of synchysite-(Ce) associated with Fe(Mn) oxides/carbonates and ankerite, (E) small batches of florencite-(Ce) in a K-feldspar groundmass, and (F) vein-like florencite-(Ce) and intergrown florencite-(Ce) and apatite associated with ankerite. *Abbreviations*: Ank: ankerite, Apt: apatite, Brt: baryte, Cal: calcite, Feld: K-feldspar, FeO: iron oxides/carbonates, Florn: florencite-(Ce), Strn: strontianite, Syn: synchysite-(Ce).

challenging because of their small size. Conversely, granular crystals of synchysite would be easier to liberate and subsequently recover. Similarly, agglomerations of 'needle-like' crystals would behave as a large particle and should also be easier to recover. No crystals of synchysite > 150 µm diameter have been seen by the authors, at Songwe Hill, or in published work on samples containing synchysite from other localities and rock types. Even samples labelled 'synchysite' in which the crystals look to be cm-size, are intergrowths of different REE fluorcarbonates (Daniel Atencio pers comm.) and there seems to be a general rule that synchysite forms small platy crystals that will be difficult to liberate during processing. This means that in addition to the properties of synchysite, the properties of the host mineral (for example, magnetic behaviour, electrical conductivity or specific gravity) will also need to be considered when processing this ore deposit.

Florencite-(Ce), the least common REE mineral, occurs as anhedral vein-like grains or as individual fine patches (Fig. 6E and F). Florencite-(Ce) grains are smaller than the other REE minerals, with a grain size up to ~30 µm and associated with all the gangue minerals.

Gangue minerals make up 90–93 wt% of the modal mineralogy. There are no significant variations in the proportion of the valuable and gangue minerals in the crushed samples P_{100} of 1700 µm, even between the ground composites P_{80} of 53 µm and 38 µm, or the size-by-size fractions of the ground composite sample P_{80} of 53 µm (Table 2). Valuable minerals are associated with all gangue minerals, particularly the major minerals, in different proportions and do not show a preferential association with one mineral. This is due to the complex nature of the ore deposit, the coarseness of the measured particles (1700 µm), and the fineness of the valuable minerals.

4.2. Liberation and mineral association

The liberation parameter is a key indicator for successful process

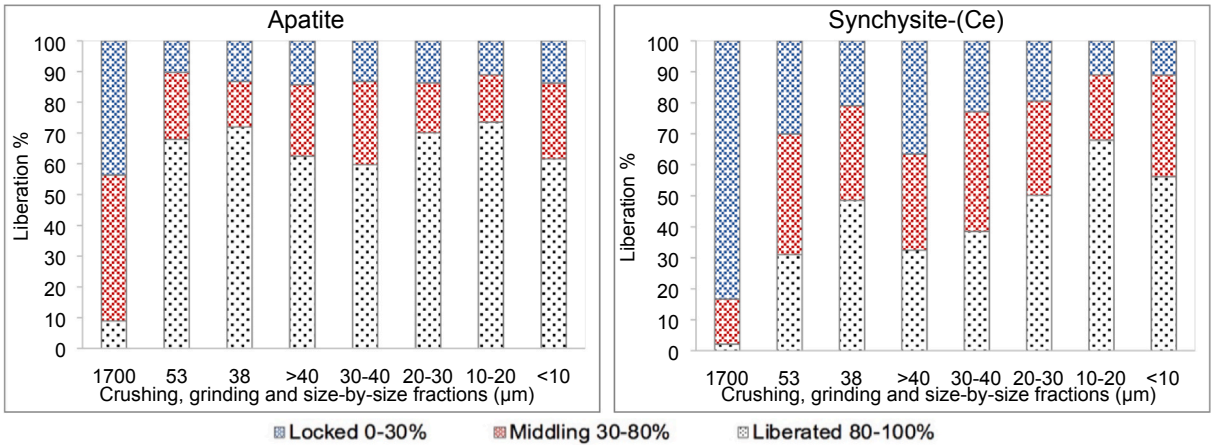

Fig. 7. Liberation degree of apatite and synchysite-(Ce) in the crushing, grinding and size-by-size fractions of the composite sample as determined by QEMSCAN®.

separation (McIvor and Finch, 1991). The degree of liberation can be improved by grinding an ore feed sample to a finer fraction, to increase the valuable mineral liberation and decrease its association with gangue minerals, hence improving the recovery and the beneficiation process.

While the results of the crushed drill core samples reveal that all the minerals of interest are not well liberated, the ground composite samples P_{80} of 53 μm and 38 μm show a significant improvement in the liberation of the valuable minerals, particularly apatite. In regard to the size-by-size fractions of the composite sample of 53 μm, the mineral liberation increases as the size fractions decreases (Fig. 7). Decreasing liberation of the valuable minerals by about 10% in the < 10 μm size fraction could be due to the tendency of these ultrafine particles to agglomerate (Pascoe et al., 2007).

Based on QEMSCAN® measurements, a maximum liberation degree of 50% for synchysite-(Ce) and 72% for apatite is achieved after fine grinding to P_{80} of 38 μm. A similar trend is also shown by the association of apatite and synchysite-(Ce) grains with the background (resin) in the size-by-size fractions, which increases as the size fraction decreases through > 40 μm and < 10 μm (Fig. 8).

The distribution of the valuable mineral mass based on the liberation degree is presented in Table 3. It is clear that a high weight percent of the target mineral mass is liberated. The mass of liberated apatite is higher than that of synchysite-(Ce) in the composites and size-by-size fractions. For example, about 3.38 wt% of 5.56 wt% of apatite and about 1.00 wt% of 3.22 wt% of synchysite-(Ce) are liberated in the composite sample P_{80} of 53 μm. This could be due to the coarse size of apatite compared to synchysite-(Ce), as evident from the automated mineralogy results (Fig. 6A-D).

4.3. Whole rock and ore minerals chemistry

4.3.1. Whole rock chemistry

The composition of the crushed drill core samples is listed in Table 4. General trends in the composition of the Songwe Hill carbonatites are discussed in Broom-Fendley et al. (2017a).

The samples are rich in REE with total rare earth oxide (TREO) contents of 1.2–2.1 wt%. Overall, Ce_2O_3 accounts for 45% of the TREO, followed by, in order of abundance: La_2O_3, 25%, Nd_2O_3 15%, Pr_2O_3 5%, Y_2O_3 4%, Sm_2O_3 2%, Gd_2O_3 2%, and other REO of about 2% (Fig. 9). Other potentially economic metals include phosphorus (1.3–2.1 wt%) and niobium (1543–3165 ppm).

As demonstrated by Broom-Fendley et al. (2017b), there is a positive linear correlation between P_2O_5 and Y_2O_3 in the carbonatite from Songwe Hill. Broom-Fendley et al., (2017b) demonstrated that apatite is the principal host of Y_2O_3 and, therefore, HREE, at this deposit.

4.3.2. Composition of the valuable minerals

The compositions of apatite, synchysite-(Ce), parisite-(Ce) and florencite-(Ce) from Songwe Hill, as analysed by EPMA, are listed in Tables 5 and 6. Further EPMA data for these minerals from Broom-Fendley et al. (2017b) are included here for comparison.

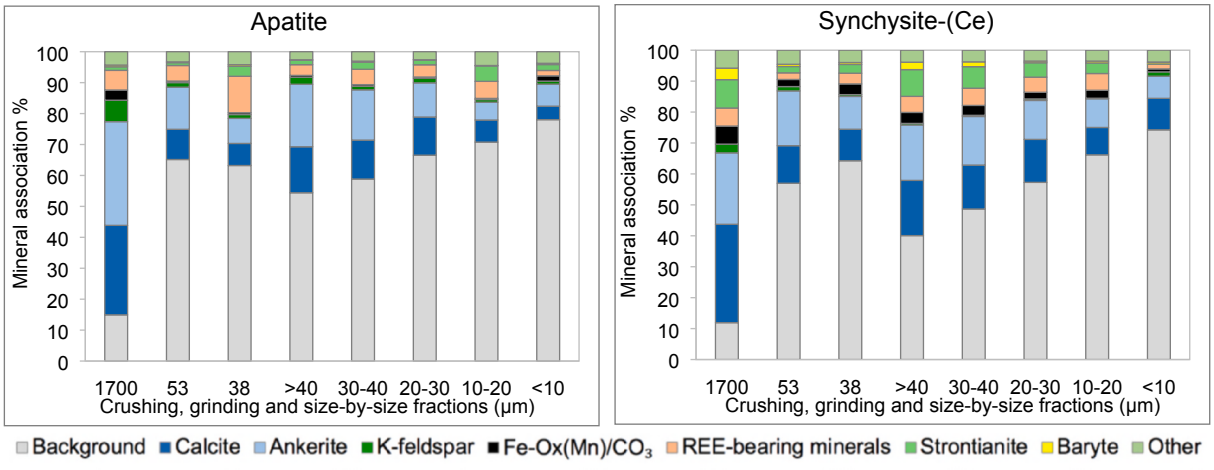

Fig. 8. Mineral association percentage of apatite and synchysite-(Ce) in the crushing, grinding and size-by-size fractions of the composite sample as determined by QEMSCAN®.

Table 3
Mineral mass distribution (wt%) of apatite and synchysite-(Ce) of the composite samples and the size-by-size fractions based on the liberation degree as determined by QEMSCAN®.

Sample		Valuable mineral	Mineral mass (wt %)	Mineral mass distribution of the valuable mineral in each liberation category (wt%)[a]		
				Locked	Middling	Liberated
Composite sample P_{80} of 53 μm		Apatite	5.56	0.57	1.21	3.78
		Synchysite-(Ce)	3.22	0.97	1.25	1.00
Composite sample P_{80} of 38 μm		Apatite	5.01	0.66	0.74	3.61
		Synchysite-(Ce)	2.69	0.56	0.82	1.31
Size-by-size fractions of the composite sample P_{80} of 53 μm	> 40 μm	Apatite	4.96	0.71	1.15	3.10
		Synchysite-(Ce)	2.68	0.98	0.83	0.87
	30–40 μm	Apatite	4.15	0.55	1.12	2.48
		Synchysite-(Ce)	3.37	0.77	1.30	1.30
	20–30 μm	Apatite	3.38	0.46	0.55	2.37
		Synchysite-(Ce)	3.12	0.61	0.95	1.57
	10–20 μm	Apatite	3.36	0.37	0.52	2.47
		Synchysite-(Ce)	3.05	0.34	0.64	2.07
	< 10 μm	Apatite	4.74	0.65	1.17	2.92
		Synchysite-(Ce)	4.25	0.47	1.40	2.39

[a] Valuable minerals are classified based on 2D mineral grain area percentage into: locked < 30%, middling 30–80%, and liberated > 80%.

Table 4
Whole-rock chemistry of the Songwe Hill carbonatite drill core samples as analysed by ICP-MS and ICP-OES.

Oxides (wt%)	Crushed drill core samples							
	PX05 + 15	PX09	PX12	PX13	PX21	PX22b	PX33	PX35
MgO	0.89	1.60	1.43	1.57	1.39	1.61	1.27	1.45
Al_2O_3	1.74	5.01	2.12	1.98	2.76	1.24	3.22	3.26
SiO_2	5.30	12.75	6.32	5.23	7.88	3.43	9.04	9.21
P_2O_5	1.91	1.24	1.61	2.10	1.52	1.35	1.29	2.01
SO_3	0.41	0.49	0.26	0.86	0.42	0.37	0.69	0.25
K_2O	0.92	2.64	1.30	1.01	1.59	0.61	1.92	2.02
CaO	37.40	19.87	32.38	27.28	27.50	29.71	23.11	27.51
MnO	1.54	3.11	2.02	2.54	2.38	2.68	2.35	2.08
FeO	8.72	19.14	10.09	15.58	14.29	15.68	20.20	12.58
SrO	1.08	0.61	0.92	1.51	1.28	1.25	1.04	0.81
(ppm)								
ZrO_2	290	349	358	436	241	211	287	416
Nb_2O_5	2125	1543	2588	2073	1846	1737	3165	2157
ThO_2	292	382	327	374	360	284	340	281
UO_2	15	12	13	11	11	9	11	12
La_2O_3	2971	3800	3348	5327	4153	3609	3765	3302
Ce_2O_3	4952	6784	5683	9748	7581	6469	7341	5897
Pr_2O_3	540	700	607	897	756	686	724	592
Nd_2O_3	1760	2352	2034	2875	2592	2384	2315	2137
Sm_2O_3	289	271	338	420	370	334	370	260
Eu_2O_3	78	88	95	111	121	94	101	97
Gd_2O_3	212	185	221	265	241	212	214	227
Tb_2O_3	25	17	23	28	26	25	27	29
Dy_2O_3	104	94	115	129	118	110	112	127
Ho_2O_3	17	12	17	22	16	20	18	21
Er_2O_3	47	40	41	54	47	51	43	51
Tm_2O_3	5	4	5	6	6	4	5	6
Yb_2O_3	32	28	29	39	36	35	33	41
Lu_2O_3	6	5	4	5	5	5	4	6
Y_2O_3	636	591	647	735	549	571	604	657
TREO	11,674	14,971	13,207	20,661	16,617	14,609	15,676	13,450

The predominant phosphate minerals are apatite and florencite-(Ce). Apatite hosts REE, ranging from trace levels (see Broom-Fendley et al., 2017b) up to 2.42 wt%, averaging 1.71 wt%. The average HREE content of apatite is 1.16 wt%, while LREE average 0.55 wt%. Florencite-(Ce) is the least common REE mineral with a total REE content of 18–30 wt%, averaging 24 wt%, predominantly LREE.

The average TREO concentration in synchysite-(Ce) and parisite-(Ce) is 50 wt% and 58 wt%, respectively (Table 6). Both are LREE-enriched, with Ce_2O_3 as the most abundant REE, followed by La_2O_3, Nd_2O_3 and Pr_2O_3, as well as minor to trace amounts of HREE. There is some variation in the degree of LREE-enrichment in synchysite-(Ce) (Table 6). However, one mineral processing flowsheet can be applied to the whole deposit as the amount of compositional variation is small and synchysite-(Ce) is consistently the main REE fluorcarbonate throughout the deposit.

The species of synchysite determines the elemental deportment of different ore minerals, as well as its magnetic susceptibility and magnetic behaviour. Synchysite-(Ce) is a diamagnetic mineral (Al-Ali et al., 2019), but there are no data on the magnetic properties of other rarer synchysite species, such as synchysite-(Y) and synchysite-(Nd). It may be possible to estimate the magnetic behaviour of these other species based on their composition and the magnetic susceptibility of Nd and Y.

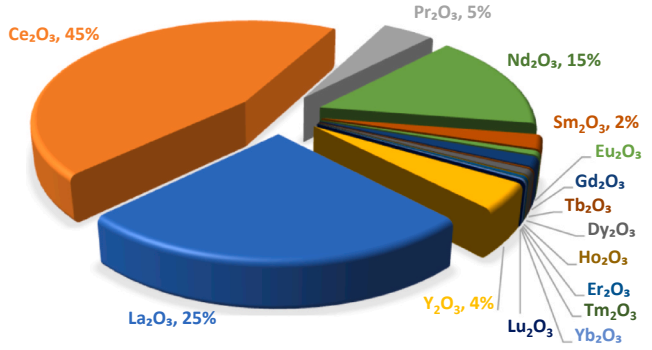

Fig. 9. Distribution of the rare earth elements within the Songwe Hill carbonatite deposit using normalised percentages. Note the data were normalised based on the average total concentration of the REO in eight crushed drill core samples in Table 4.

In nature, other REE occur in synchysite, especially other mid and light REE in synchysite-(Ce) and synchysite-(Nd), and mid and heavy REE in synchysite-(Y). The molar magnetic susceptibility of Y (2.359×10^{-3} $cm^3\ mol^{-1}$) is much lower than the molar magnetic susceptibility of Nd (74.5×10^{-3} $cm^3\ mol^{-1}$), and even lower than Ce (31.4×10^{-3} $cm^3\ mol^{-1}$) (Martienssen, 2005). By comparing the composition of these two minerals with synchysite-(Ce), we can predict that synchysite-(Y) would behave as a diamagnetic mineral, while synchysite-(Nd) as a paramagnetic mineral.

4.3.3. REE mass balance

As previously noted, Broom-Fendley et al., (2017b) demonstrated that apatite at Songwe Hill is HREE-rich, relative to most other carbonatite-hosted REE deposits. In order to investigate the mass balance of the different REE across the available REE-bearing minerals, the average concentration for each REE has been normalised by its modal abundance as determined by QEMSCAN® analyses (Fig. 10). Other minerals, such as calcite and fluorite, are only capable of hosting the REE in small amounts, but these may also be significant given their high modal abundance. To calculate the mass balance for these phases, trace element data was taken from Broom-Fendley et al. (2017b, and unpublished data).

Owing to the low concentration of HREE in synchysite-(Ce), the presented mass-balance data become unavoidably less reliable for the heavier REE. Indeed, Eu, Tb, Ho, Er, Tm, Yb, and Lu are not included in Fig. 10 as these elements are below detection in EPMA analyses of synchysite-(Ce) and apatite. Trace element analyses of synchysite-(Ce), using LA ICP MS, are beyond the scope of this study and would be challenging to undertake owing to their small size and platy habit.

Synchysite-(Ce) hosts most of the LREE containing 88% of the available Ce in the rock, with florencite-(Ce) predominantly accounting for 11% and apatite about 1%. The importance of synchysite-(Ce) as a REE host decreases for heavier REE as apatite becomes the dominant REE-bearing mineral. For all REE heavier than Gd, apatite is the most important REE host. Interestingly, however, for the two REE where data are available in both synchysite-(Ce) and apatite (Dy and Y), synchysite-(Ce) still accommodates > 25% of the whole-rock HREE content. Thus, while apatite is an important phase for hosting the REE, synchysite-(Ce) remains an important valuable mineral. Gangue phases such as calcite and fluorite contain a negligible amount of LREE, and only amount to ~5% of the Y contents. For the purposes of tracking synchysite-(Ce) and apatite contents during mineral processing tests, the respective contents of Ce and Y are sufficiently robust proxies.

5. Mineralogical implications for minerals processing

Characterising the modal mineralogy, liberation, mineral associations, average grain size, and mass-size distribution are key parameters to improve the mineralogical understanding of an ore deposit. They are also key parameters for identifying the potential metallurgical beneficiation route and to optimise recovery of the target minerals. Herein we discuss how these mineralogical characteristics can be utilised to predict behaviour in mineral processing and present a possible flowsheet option to process the Songwe Hill deposit.

Table 5
Average compositions for apatite and florencite-(Ce) from the Songwe Hill carbonatite, as determined by EPMA (Broom-Fendley et al., 2017b).

Oxides (wt %)	Apatite $Ca_5(PO_4)_3F$				Florencite-(Ce) $CeAl_3(PO_4)_2(OH)_6$			
	5 spot points				6 spot points			
	Min	Max	Avg	σ	Min	Max	Avg	σ
Al_2O_3					27.17	30.22	28.53	1.01
SiO_2	0.01	0.01	0.01	0.00	0.08	0.21	0.11	0.05
P_2O_5	39.79	41.30	40.63	0.57	22.19	25.97	24.43	1.28
SO_3	0.04	0.25	0.09	0.11				
Na_2O	0.46	0.63	0.52	0.07	–	0.03	0.01	0.01
MgO					–	0.03	0.02	0.01
CaO	52.58	54.12	53.59	0.61	0.89	3.42	1.68	0.96
MnO	0.06	0.19	0.13	0.09				
FeO	0.04	0.28	0.15	0.12	0.56	2.34	1.10	0.65
SrO	1.24	1.69	1.46	0.17				
Y_2O_3	0.54	1.07	0.86	0.20	–	–	–	
La_2O_3	0.05	0.12	0.09	0.05	6.99	10.44	8.69	1.21
Ce_2O_3	0.06	0.34	0.17	0.11	9.42	13.75	12.27	1.66
Pr_2O_3	0.01	0.08	0.04	0.03	0.88	2.02	1.35	0.47
Nd_2O_3	0.11	0.37	0.21	0.10	0.72	3.42	1.79	1.15
Sm_2O_3	0.03	0.05	0.04	0.01	–	0.15	0.05	0.06
Gd_2O_3	0.11	0.19	0.16	0.03	–	–	–	
Dy_2O_3	0.10	0.20	0.15	0.04				
ThO_2	0.03	0.05	0.04	0.01	–	–	–	
F	4.60	5.06	4.88	0.20				
Cl	0.01	0.01	0.01	0.00				
-O = F, Cl	1.94	2.13	2.04	0.08				
Total	97.93	103.88	101.19		68.90	92.00	80.02	
Atoms per formula unit (apfu) on the basis of 12.5 and 11 anions for apatite and florencite-(Ce), respectively.								
Al					3.279	2.925	3.079	
Si	0.001	0.001	0.001		0.008	0.017	0.010	
P	2.910	2.959	2.941		1.924	1.805	1.894	
S	0.001	0.016	0.005					
Na	0.076	0.105	0.086		–	0.005	0.002	
Mg					–	0.004	0.002	
Ca	4.842	5.009	4.910		0.098	0.301	0.164	
Mn	0.001	0.014	0.006					
Fe	0.001	0.020	0.008		0.048	0.161	0.084	
Sr	0.062	0.084	0.072					
Y	0.025	0.050	0.040		–	–	–	
La	0.000	0.004	0.002		0.264	0.316	0.294	
Ce	0.002	0.011	0.005		0.353	0.413	0.412	
Pr	0.000	0.002	0.001		0.033	0.060	0.045	
Nd	0.003	0.011	0.006		0.026	0.100	0.058	
Sm	0.001	0.001	0.001		–	–	–	
Gd	0.003	0.005	0.004		–	–	–	
Dy	0.003	0.005	0.004		–	–	–	
Th	0.001	0.002	0.002		–	–	–	
F	1.231	1.375	1.320					
Cl	0.001	0.001	0.001					

Note: Blank cells denote elements not analysed and – denotes elements below the limit of detection. UO_2 below 0.01 wt% in all analyses. Eu_2O_3 and Tb_2O_3 below detection in all analyses.

5.1. Gravity separation

Gravity concentration is widely used due to low capital and operating costs, an absence of chemical reagents and a lack of excessive heating requirements (Falconer, 2003). For efficient separation, a significant density contrast between valuable and gangue minerals is required, and separation efficiency increases with increased particle size (Gupta and Yan, 2016; Wills and Finch, 2016).

Table 6
Average compositions for synchysite-(Ce) and parisite-(Ce) from the Songwe Hill carbonatite, as determined by EPMA.

Oxides (wt%)	Synchysite-(Ce) $CaCe(CO_3)_2F$				Synchysite-(Ce) $CaCe(CO_3)_2F$				Parisite-(Ce) $CaCe_2(CO_3)_3F_2$			
	21 spot points				178 spot points[a]				7 spot points[a]			
	Min	Max	Avg	σ	Min	Max	Avg	σ	Min	Max	Avg	σ
CaO	14.00	17.83	16.70	1.10	14.33	18.11	16.36	0.73	9.30	11.41	10.37	0.80
MnO					–	0.09	0.01	0.02	–	0.02	0.00	0.01
FeO					–	2.29	0.36	0.55	–	0.25	0.06	0.09
SrO	–	–	–		–	2.52	0.35	0.30	0.40	1.02	0.75	0.25
BaO	–	–	–		–	2.74	0.05	0.22	–	0.79	0.29	0.27
Y_2O_3	–	2.06	0.61	0.68	–	2.70	0.56	0.47	–	0.36	0.07	0.13
La_2O_3	8.20	22.23	12.44	3.50	7.54	20.62	13.36	3.07	18.03	23.45	21.42	1.89
Ce_2O_3	20.18	27.75	24.21	1.98	18.76	28.62	24.47	1.40	27.01	28.79	27.92	0.72
Pr_2O_3	1.35	3.25	2.35	0.48	1.74	4.32	2.48	0.37	2.04	2.71	2.33	0.23
Nd_2O_3	3.95	12.13	7.67	1.73	4.23	12.97	8.29	1.93	4.80	7.83	5.80	1.05
Sm_2O_3	0.35	1.71	0.85	0.41	0.15	2.57	0.93	0.42	0.23	0.54	0.34	0.13
Eu_2O_3	–	–	–		–	0.53	0.14	0.10	–	0.06	0.03	0.03
Gd_2O_3	–	1.05	0.59	0.25	–	1.88	0.30	0.31	–	–	–	
Dy_2O_3	–	–	–		–	0.49	0.16	0.11	–	0.11	0.02	0.04
ThO_2	0.19	6.73	1.29	1.35	0.02	2.82	0.80	0.51	0.08	0.73	0.35	0.24
F*	5.59	6.31	5.89	0.17	5.47	6.11	5.89	0.11	5.46	7.03	6.33	0.74
CO_2*	25.90	29.25	27.28	0.80	25.36	28.30	27.27	0.53	23.12	26.12	24.76	1.03
-O = F*	2.35	2.66	2.48	0.07	2.31	2.57	2.48	0.05	2.30	2.96	2.67	0.31
Total	92.61	104.38	97.40		92.18	104.22	99.55	1.95	94.76	101.07	98.39	
Atoms per formula unit (apfu) on the basis of 7 and 11 anions for synchysite-(Ce) and parisite-(Ce), respectively.												
Ca	0.752	0.728	0.79		0.956	0.806	0.930		0.903	1.079	0.990	
Mn					–	0.003	0.000		–	0.001	0.000	
Fe					–	0.080	0.016		–	0.019	0.004	
Sr	–	–	–		–	0.061	0.011		0.021	0.054	0.039	
Ba	–	–	–		–	0.045	0.001		–	0.027	0.010	
Total	0.752	0.728	0.79		0.956	0.995	0.958		0.924	1.18	1.043	
Y	–	0.042	0.01		–	0.060	0.016		–	0.017	0.003	
La	0.152	0.313	0.20		0.173	0.316	0.261		0.575	0.766	0.706	
Ce	0.371	0.387	0.39		0.428	0.435	0.475		0.888	0.935	0.912	
Pr	0.025	0.045	0.04		0.039	0.065	0.048		0.066	0.085	0.076	
Nd	0.071	0.165	0.12		0.094	0.192	0.157		0.160	0.242	0.184	
Sm	0.006	0.022	0.01		0.003	0.037	0.017		0.007	0.016	0.011	
Eu	–	–	–		–	0.008	0.003		–	0.002	0.001	
Gd	–	0.013	0.01		–	0.026	0.005		–	–	–	
Dy	–	–	–		–	0.007	0.003		–	0.003	0.000	
Th	0.002	0.058	0.01		0.000	0.027	0.010		0.002	0.015	0.007	
Total	0.627	1.045	0.79		0.737	1.173	0.995		1.698	2.081	1.9	
TREE:Ca	1:1	1:1	1:1		1:1	1:1	1:1		2:1	2:1	2:1	

Note: * calculated by stoichiometry, blank cells denote elements not analysed and – denotes elements below the limit of detection. Tb and U were also analysed, but below detection in all samples.

[a] Broom-Fendley et al. (2017b).

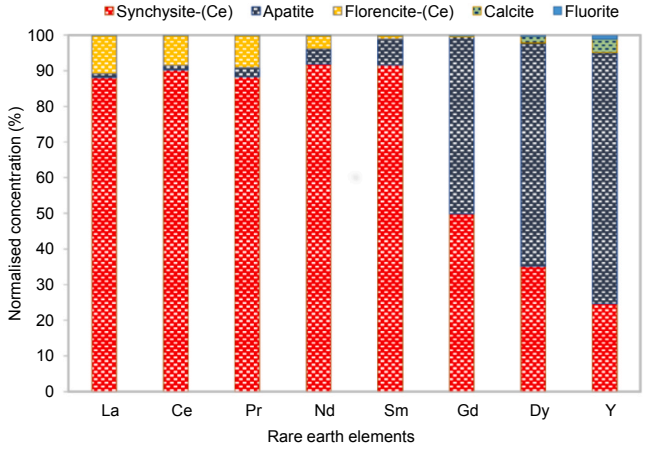

Fig. 10. Mass balance of the REE within the valuable minerals and some gangue minerals of the Songwe Hill carbonatite samples. Data were normalised based on the total concentration of each respective element in apatite, synchysite-(Ce), florencite-(Ce), calcite and fluorite.

Table 7 summarises the key physical characteristics of the valuable minerals at Songwe Hill. It is evident from these data that there is only a small difference in specific gravity between apatite (major valuable mineral) and ankerite and calcite (major gangue minerals). The specific gravity of synchysite-(Ce) is higher than the major gangue minerals.

Examination of mineral density alone is not sufficient to fully evaluate the potential for gravity separation as it does not account for the size or density of the particles in which the minerals of interest are contained. Using quantitative mineralogical data, it is possible to examine the distribution of particles by both size and density (Pascoe et al., 2007) and to relate this to recovery of REE-bearing minerals. For this study, quantitative mineralogical data for the 8 samples stage crushed to −1700 μm were used. Analyses are based on the properties of 172,732 particles examined.

Fig. 11 shows the mass distribution of REE-bearing minerals in particle density classes in comparison to the overall mass distribution. REE-bearing minerals are concentrated in slightly denser particles compared to the overall sample, though the difference is < 1.5 g·cm^{-3} (Fig. 11). Synchysite-(Ce) is most prominently represented in the denser classes and the density of particles containing apatite are similar to the overall mass distribution. These findings support the analysis of mineral properties given in Table 7.

For gravity separation to be effective there must be a large

Table 7
Mineralogical composition of the major and minor valuable and gangue minerals of the Songwe Hill carbonatite deposit along with some of their physical characteristics (Tickell, 2011; Jordens et al., 2013; Krishnamurthy and Gupta, 2016; Wills and Finch, 2016; Al-Ali et al., 2019).

Mineral name		Mineral abundance (wt%)	Specific gravity[a]	Magnetic response		
				Ferromagnetic	Paramagnetic	Diamagnetic
Valuable	Apatite	5.56	3.2			X
	Florencite-(Ce)	0.60	3.6	N/A		
	Synchysite-(Ce)	3.22	4.0			X
Gangue	Ankerite	30.34	3.1		X	
	Baryte	0.98	4.48			X
	Calcite	27.04	2.7			X
	Fe-Ox/CO_3 [b]	12.69	3.8–5.3		◄-------	
	K-feldspar	9.52	2.6			X
	Muscovite	1.87	2.8			X
	Strontianite	1.17	3.8			X

N/A not available.
[a] Data from www.webmineral.com.
[b] Including magnetite, jacobsite, titaniferous magnetite (ferromagnetic) and/or siderite, hematite, goethite and limonite (paramagnetic).

difference in density between the minerals of interest and gangue minerals, within size ranges which are suitable for gravity separation processes. The modest density differences shown in Fig. 11 indicate that gravity separation would be difficult. To provide more detailed analysis both size and density classes were considered. Fig. 12 shows the mass distribution of REE-bearing minerals within size-density classes. The majority of the analysed sample is relatively coarse, with over 91% of the particles are over 180 μm. As in Fig. 11, there is an upgrade of REE-bearing minerals in the density range of 3.0–4.0 g·cm^{-3}. However, the largest upgrades are in the smallest size fractions which would indicate that gravity separation would be difficult.

In Fig. 13A the upgrade potential of REE-bearing minerals for size-density classes is superimposed on the mass distribution of REE-bearing minerals. In Fig. 13B, a similar approach is adopted for the expected total rare earth element (TREE) grades. TREE grades are calculated from EPMA data reported in Section 4.3.2. A limitation to this approach is that there is no information on the TREE content of bastnäsite and monazite. However, these minerals represent only 0.02–0.04% of the mineral mass in the samples and so there is minimal error introduced by not considering these minerals.

In Fig. 13A and B, points with a value above 1 (yellow-green) have a higher grade than the overall feed grade (i.e. positive upgrade). There is little mass of TREE within REE-bearing minerals in finer fractions where the greatest upgrade would be possible (Fig. 13). Further grinding of the sample should increase particles in the range of greatest upgrading. However, Fig. 13B highlights the narrow density difference between TREE enriched classes and TREE depleted ones. As the density differences between enriched and depleted classes is low, gravity separation would be difficult.

Fig. 13 also shows that there is some limited potential to pre-concentrate the +500 μm size classes, which could be achieved using dense medium separation. However, the level of upgrade would be

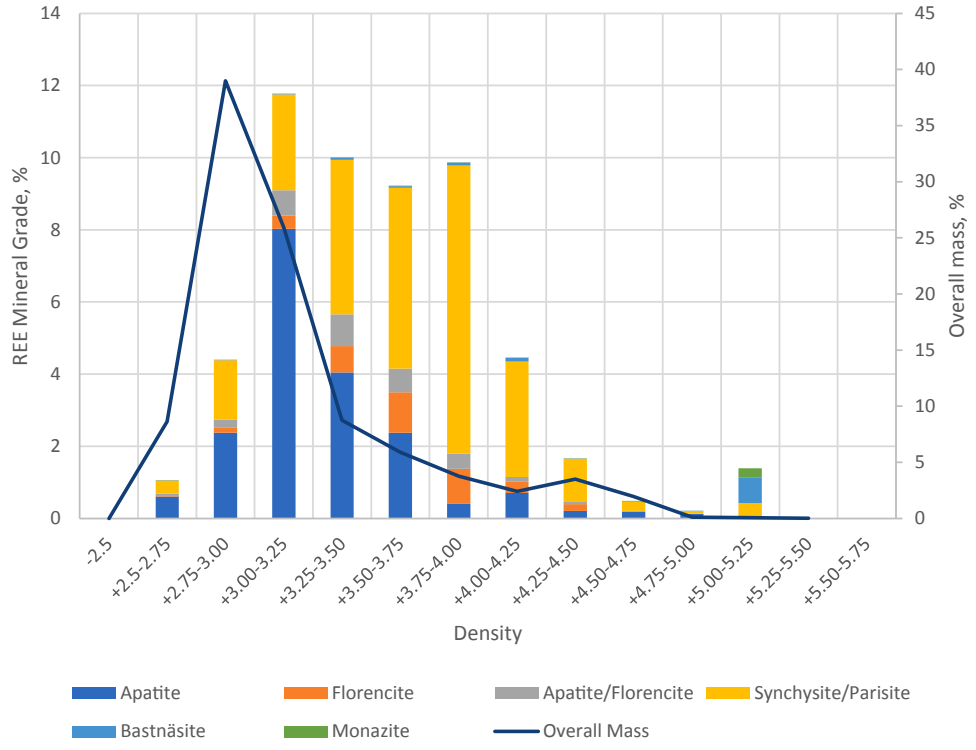

Fig. 11. Mass distribution of REE-bearing minerals across density ranges for the crushed drill core sample P_{100} of 1700 μm. Overall mass distribution superimposed/(solid line) for comparison.

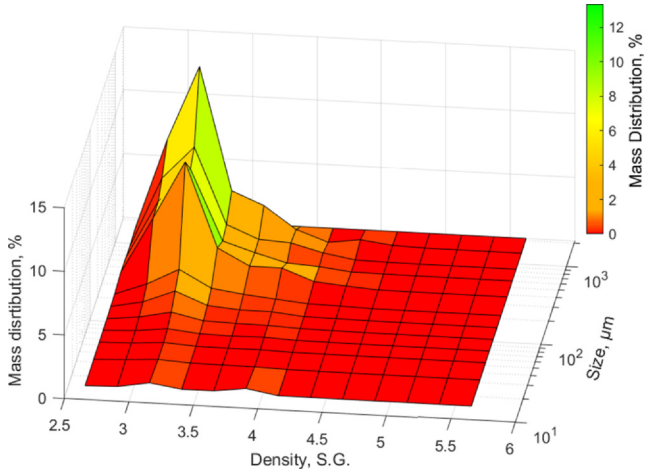

Fig. 12. Mass distribution of REE-bearing minerals across size and density classes.

limited. For example, a separation at 3.0 g·cm^{-3} would increase the grade of REE-bearing minerals in the +500 μm size range from 1.5% to 2.0% with a recovery of 60% of REE-bearing minerals and overall mass pull of 44%.

Overall, the quantitative mineralogical data indicates that gravity separation would be unlikely to be an effective means of processing the ore to upgrade REE-bearing minerals.

5.2. Grinding

Grinding is the most energy-consuming operation in a mineral processing flowsheet, particularly for a complex and fine-grained deposit (Wills and Finch, 2016). Grinding aims to enhance the liberation of the target minerals and remove the associated gangue minerals.

The mineral liberation analyses of Songwe Hill samples (Figs. 7 and 8), demonstrate that the valuable minerals in the crushed drill core samples P_{100} of 1700 μm are poorly liberated and associated with all gangue phases. Grinding to P_{80} of 53 μm enhanced the liberation of valuable minerals, especially apatite, and decreased their associations with other gangue minerals. Further grinding to P_{80} of 38 μm greatly enhanced the liberation of valuable minerals, particularly for synchysite-(Ce), although these minerals are still not fully liberated and remain locked by the host gangue particles. However, fine grinding to P_{80} of 38 μm generated very fine particles (< 10 μm) of about 40 wt% (Fig. 14) which are problematic for physical separation. Thus, it is recommended to process Songwe Hill deposit at a grinding size P_{80} of 53 μm to minimise losing valuable phases to the tailings.

5.3. Particle size analysis, classification and desliming

Particle size analysis, classification and desliming of an ore deposit prior to undertaking a mineral processing test may be required to enhance separation efficiency. Particle size analysis is important for determining the size range of particles after the grinding step. A classification step may be required to split the bulk ore sample into different products based on particle size (e.g. fine, medium and coarse products) or grade (e.g. high-grade and low-grade products), to be processed separately using the same or different methods and conditions. Desliming may be applied to remove ultrafine and very fine fractions from the ore sample to increase the efficiency of the beneficiation process.

The particle size distribution at Songwe Hill show that the amounts of classified sample slightly vary from one size fraction to another, between 10 and 21%, except the < 10 μm size fraction which contains a notable proportion (~36 wt%) of the whole ground composite sample P_{80} of 53 μm (Table 8).

Automated mineralogical data indicate that valuable minerals are equally distributed between all size fractions. Adding a desliming step (i.e. removing the < 10 μm fraction), prior to conducting a processing test, will adversely affect the recovery of the whole process. Such a step would result in a loss of approximately 23% and 26% of the total apatite and synchysite-(Ce) contents, respectively. However, it may be possible to classify the ore deposit into different products based on the particle size, and separately process the very fine size fraction product (i.e. < 10 μm).

5.4. Magnetic separation

Magnetic separation is widely used to beneficiate REE deposits by separating minerals with different magnetic properties (Jordens et al., 2013; Krishnamurthy and Gupta, 2016). It can be used to concentrate valuable diamagnetic minerals, recover all magnetic minerals (ferromagnetic or paramagnetic), separate ferromagnetic from paramagnetic minerals or selectively separate paramagnetic particles based on their

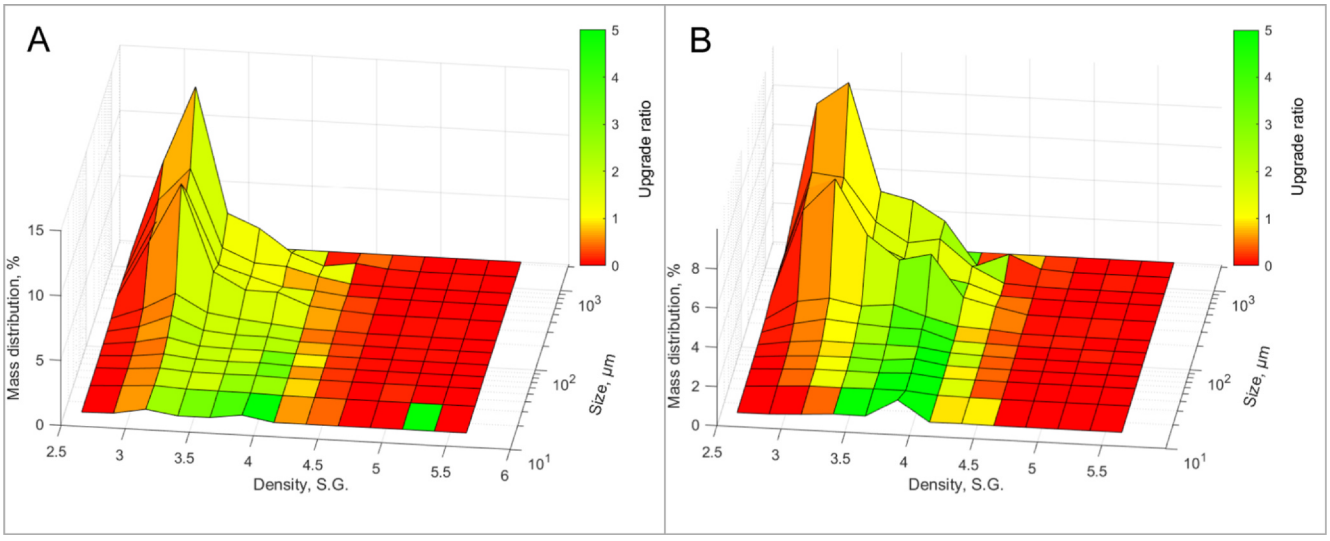

Fig. 13. Mass distribution of (A) REE-bearing minerals and (B) TREE across size and density classes. Upgrade potential within size and density classes is superimposed with change in colour. Yellow-green represents a positive upgrade and orange-red a negative upgrade. (For interpretation of the references to colour in this figure legend, the reader is referred to the web version of this article.)

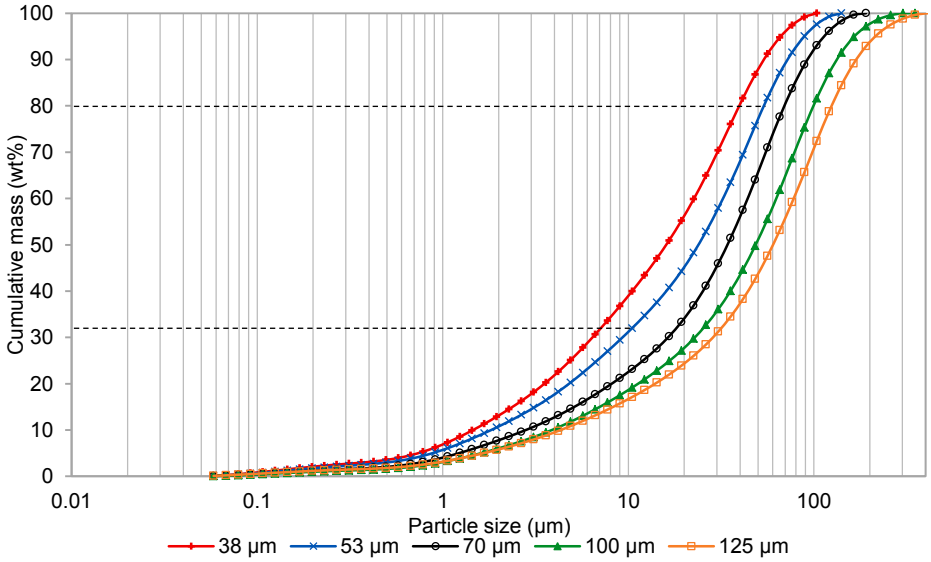

Fig. 14. Particle size distribution of the composite sample at different grinding size, as measured by laser size diffraction, showing the size passing fraction of P_{80} and the amount of very fine particles (< 10 μm).

Table 8
Particle size distribution and normalised abundance of apatite and synchysite-(Ce) in each size fraction of the ground composite sample P_{80} of 53 μm. Data were normalised based on the total content of apatite and synchysite-(Ce) within all size fractions as determined by automated mineralogy.

Size fraction (μm)	Fraction weight (wt%)	Apatite (%)	Synchysite-(Ce) (%)
> 40	17	24.09	16.27
30–40	10	20.16	20.46
20–30	16	16.42	18.94
10–20	21	16.32	18.52
< 10	36	23.02	25.80

The calculated head sample is approximately 75 g.

magnetic susceptibilities at a particular magnetic field strength.

The Songwe Hill carbonatite deposit consists of a considerable amount of paramagnetic/ferromagnetic gangue minerals including ankerite (30 wt%) and iron oxides/carbonates (13 wt%), (Table 2). Iron oxides/carbonates include magnetite, jacobsite, titaniferous magnetite, siderite, hematite, goethite and limonite which behave as ferromagnetic and paramagnetic minerals and have a strong association with ankerite in most samples (Williams, 2019). Apatite and synchysite-(Ce) are both diamagnetic (Al-Ali et al., 2019; Table 7). Thus, the diamagnetic nature of the target minerals and the presence of paramagnetic gangue minerals means that wet high-intensity magnetic separation could concentrate ore from Songwe Hill and reject a high proportion of gangue minerals.

The identity of the REE fluorcarbonate is important when considering magnetic separation because although synchysite is diamagnetic, parisite and bastnäsite, with their increasing proportions of REE are more magnetic and will respond differently during magnetic separation.

Mineralogical characteristics, such as mineral grain size, liberation and association need to be taken into account when considering magnetic separation. For instance, large and well liberated synchysite-(Ce) grains are easy to separate from paramagnetic minerals such as ankerite (Fig. 15A), but small and poorly liberated synchysite-(Ce) grains associated with ankerite or iron oxides may behave as paramagnetic particles (Fig. 15B). For example, apatite and synchysite-(Ce) are highly associated with ankerite of about 34% and 23%, respectively in the composite crushed sample P_{80} of 1700 μm (Fig. 8). This association decreases in the composite sample P_{80} of 53 μm to 14% (apatite) and 18% (synchysite) (Fig. 8). Thus, these minerals could be recovered to the magnetic product and hence losing REE.

A further consideration regarding the magnetic properties of the REE fluorcarbonates is the effect of syntaxial intergrowths. Syntaxial intergrowths are a common feature among REE fluorcarbonate minerals. When synchysite is syntaxially intergrown with parisite and/or bastnäsite, it may behave as a paramagnetic particle. An example of synchysite-(Ce) associated with paramagnetic minerals is the Springer Lavergne carbonatite deposit in Ontario, Canada (Table 1). Synchysite-(Ce) is the only REE mineral in this deposit and it mostly occurs as fine-grained clusters intimately associated with iron oxides and ankerite. Other gangue minerals are K-feldspar, pyroxene/amphibole, pyrite and quartz (Mariano and Mariano, 2012; Deng and Hill, 2014). Thus, coarse grinding followed by a magnetic separation will recover the poorly liberated synchysite-(Ce) with the host magnetic particles (iron oxides and ankerite) to the magnetic product. This process would pre-concentrate the deposit from diamagnetic gangue minerals such as K-feldspar and quartz.

5.5. Froth flotation

Froth flotation has found prominence as a selective process which can separate chemically-similar minerals such as apatite and calcite in complex and low-grade ore bodies (Klimpel, 1998). It is an efficient technique to process fine-grained ore deposits, where the average grain size to achieve high liberation is too small for physical processing techniques such as gravity concentration (Kelly and Spottiswood, 1982; Santana et al., 2008; Wills and Finch, 2016).

Froth flotation has been widely employed for the beneficiation of igneous phosphates due to the well-crystallised nature and inherent low porosity of apatite compared to apatite in sedimentary phosphates (Kawatra and Carlson, 2014). It is also largely applied for processing REE deposits, particularly beneficiation of bastnäsite from carbonate gangue (Yu and Aghamirian, 2015; Krishnamurthy and Gupta, 2016). The Songwe Hill carbonatite deposit is rich in synchysite-(Ce), but there are no data available on the surface behaviour of synchysite-(Ce). Zeta potential measurements conducted under different chemical reagents and conditions suggest that Ca-bearing REE fluorcarbonate minerals behave in a similar way to bastnäsite (Owens et al., 2018). Thus, it may be possible to process synchysite-(Ce) by froth flotation using the same chemical reagents that have been used to process bastnäsite-(Ce). Consequently, froth flotation is considered to be a favourable technique

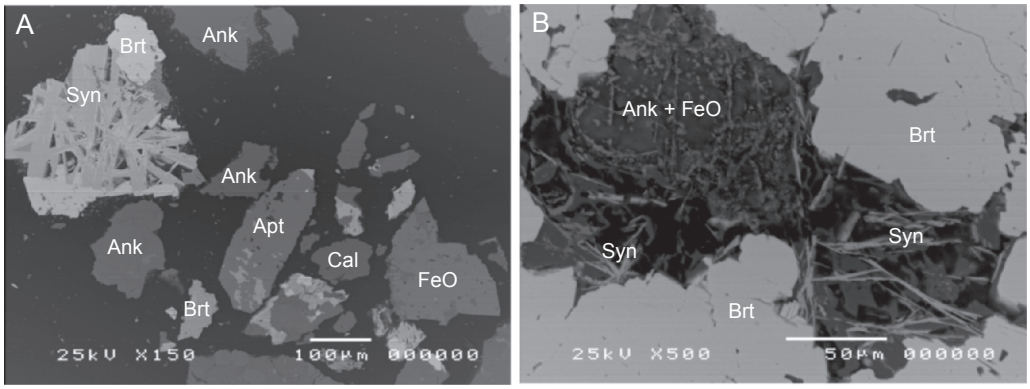

Fig. 15. Backscattered electron (BSE) images illustrating the mineralogical characteristics of the Songwe Hill ore deposit (A) accumulation of large granular (lath-shaped) synchysite-(Ce) crystals associated with baryte and (B) fine acicular (needle-like) synchysite-(Ce) crystals embedded within paramagnetic ankerite and iron oxide/carbonate groundmass. *Abbreviations*: Ank: ankerite, Apt: apatite, Brt: baryte, Cal: calcite, FeO: iron oxides/carbonates, Syn: synchysite-(Ce).

for processing the Songwe Hill deposit.

Different reagent schemes can be employed to beneficiate ore from Songwe Hill. One such possibility is a fatty acid collector, which is typically a mixture of oleic and linoleic acid, at around pH ~ 10 (Guimarães et al., 2005; Kawatra and Carlson, 2014; Fuerstenau et al., 1992; Krishnamurthy and Gupta, 2016). Various hydroxamates, dicarboxylic acids and organic phosphoric acid esters have also been widely used as collectors for recovering REE minerals, such as bastnäsite, synchysite, fergusonite and apatite (Pradip and Fuerstenau, 1991; Bulatovic, 2010; Yu and Aghamirian, 2015; Jordens et al., 2016). Rice bran and soybean bran oils are successfully utilised as apatite collectors in processing igneous phosphate deposits (Guimarães et al., 2005). Corn starch is utilised to depress carbonate and iron oxides at alkaline conditions because it is soluble in water and has a higher affinity to calcite than apatite (Leal Filho et al., 2000; Guimarães et al., 2005). Sodium silicate is employed for both igneous and sedimentary phosphate flotation to depress calcite and silicate gangue minerals (Dho and Iwasaki, 1990; Yu and Aghamirian, 2015; Jordens et al., 2016). Lignin sulphonate ($C_{20}H_{26}O_{10}S_2$) is a water-soluble anionic reagent that has been used as a depressant for calcite and baryte in the flotation of bastnäsite ore with a fatty acid collector (Fuerstenau et al., 1982; Pradip and Fuerstenau, 2013).

To evaluate the feasibility of applying flotation as a processing technique for this material the surface area of exposed REE-bearing minerals for flotation was estimated from quantitative mineralogical data. Specifically, the false colour PMA mineral map images generated by QEMSCAN® were analysed using a custom MATLAB® R2020a script to calculate the distribution of minerals on the boundary of particles. As the sample used for QEMSCAN® is a cut section, pixels on the boundary can be considered to be exposed for the purposes of flotation analysis.

Using the boundary mineral distribution data, a number of theoretical grade recovery (TGR) curves were generated. These TGR curves represent the predicted recovery for two flotation scenarios. In the first scenario, synchysite-(Ce) and bastnäsite are the target minerals. Though, as the ratio of synchysite-(Ce):bastnäsite by mineral mass abundance is 215:1, it can assumed that synchysite-(Ce) is the only target mineral.

The second scenario was to assume targeting of all REE-bearing minerals (principally, synchysite-(Ce) and apatite). The TGRs focus on LREO and HREO which were calculated from EPMA data as in Section 5.1. It should be noted that for the purposes of mass balancing and calculation of recovery the REO content of fluorite and calcite have not been considered due to the expected low concentrations. As shown in Fig. 10, the expected LREO and HREO (including Y) mass within these minerals is 1.2% and 7.4% respectively. It is not anticipated that these low concentrations will affect the overall trends reported. The specific methodology for generating TGR curves is summarised below.

1. Extract particle data from QEMSCAN® generated PMA mineral map false colour images and generate database of particles.
2. Calculate abundance of minerals on individual particle surfaces using MATLAB® R2020a script.
3. Sort particles from high to low surface grade of either synchysite-(Ce)/bastnäsite or all REE-bearing minerals.
4. Use mineral masses and LREO and HREO mineral content estimated from EPMA data to determine grade of LREO and HREO of

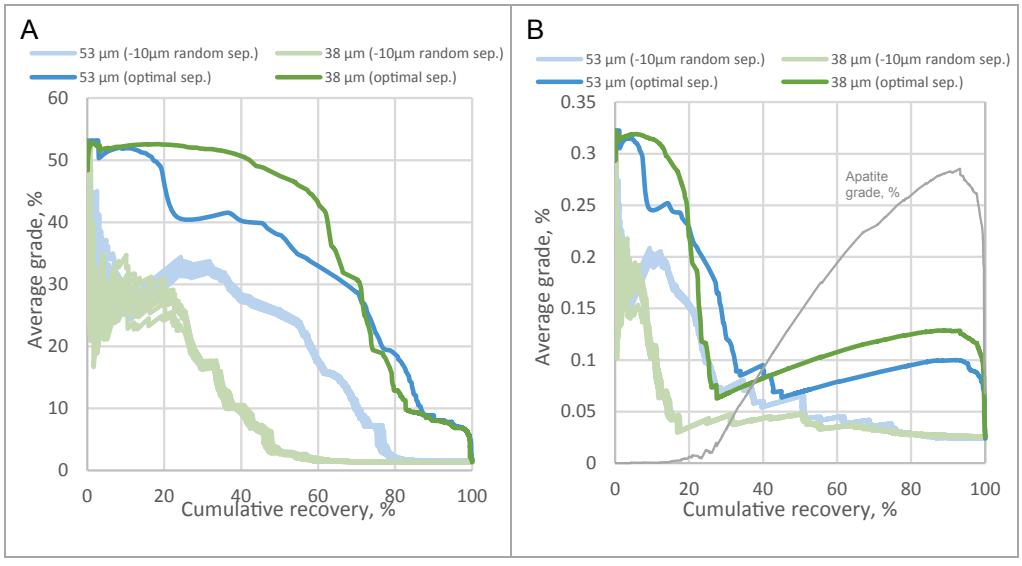

Fig. 16. Theoretical grade recovery curves of (A) LREO and (B) HREO for grind sizes of P_{80} 53 µm and P_{80} 38 µm based on data generated by QEMSCAN®. Curves created based on fraction of synchysite-(Ce) exposed on the surface. Darker lines represent perfect separation from high to low surface exposure. Lighter lines represent a simulation of the effects of slimes on flotation with random recovery of −10 µm particles. Ten random simulations were undertaken to evaluate the range of TGR.

individual particles.
5. Calculate average grade and cumulative recovery using cumulative mass data of individual particles.

5.5.1. Flotation targeting synchysite-(Ce) and bastnäsite

Fig. 16 shows TGR curves assuming synchysite-(Ce) and bastnäsite are targeted during flotation. Darker lines represent TGRs assuming all particles are selectively recovered. The paler lines represent the TGRs assuming +10 μm particles are selectively recovered and −10 μm particles are randomly recovered (10 simulations are represented). Fig. 16A shows results for LREO and Fig. 16B shows results for HREO.

LREO are more effectively recovered than HREO when targeting synchysite-(Ce) which is expected given the dominance of LREO in synchysite-(Ce) (Fig. 16). When all particles are selectively recovered 38 μm is the optimal grind size. However, when the effects of slimes are simulated (random recovery of −10 μm fraction), the 53 μm grind size is preferable. Fig. 16A shows that a reasonable upgrade of LREO can be achieved. However, Fig. 16B shows that if targeting synchysite-(Ce), HREO are not effectively recovered. This has implications for the profitability of the process given the relative value of HREO compared to LREO.

The trend in Fig. 16A generally follows the expected behaviour of decreasing grade with increasing recovery. Where there are small increases in grade observed with increased recovery this is explained by the methodology for generating the TGRs which are based on particles sorted by surface exposed synchysite-(Ce)/ bastnäsite, and not the grade of the entire particle. Where particles are not well liberated, a high surface grade does not always result in a high overall grade. Also where particles contain significant proportions of bastnäsite the LREO content drops due to the lower mineral content. Example images of such particles are shown in Fig. 17.

The trend in Fig. 16B, does not generally follow expected behaviour of decreasing grade with increasing recovery. The grade is initially relatively high, as synchysite-(Ce) contains HREO. As particles with lower grades of synchysite-(Ce) are recovered the grade of HREO declines. Between 20 and 30% recovery of HREO, the grade of HREO increases, this can be explained by the increased grade of apatite in the concentrate at this point. This can be seen in Fig. 16B which shows the grade of apatite for the P_{80} 38 μm sample. So, in this case, the primary explanation for the trend is that the majority of HREOs are contained within apatite, which is not targeted and has low association with synchysite-(Ce); quantitative mineralogical results show overall association of < 1% for P_{80} 38 μm sample. The trend could be considered more analogous to recovery curves for gangue minerals.

5.5.2. Flotation targeting all REE-bearing minerals

Fig. 18 shows TGR curves assuming all REE-bearing minerals are targeted during flotation (mainly apatite and synchysite-(Ce)). Darker lines represent TGRs assuming all particles are selectively recovered. Paler lines represent the TGRs assuming +10 μm particles are selectively recovered and −10 μm particles are randomly recovered (10 simulations are represented). Fig. 18A show results for LREO and Fig. 18B shows results for HREO.

Fig. 18 shows that HREO are more effectively recovered than LREO when targeting all REE-bearing minerals. This is a result of the larger abundance of highly liberated HREO-rich apatite which are preferentially recovered to synchysite-(Ce). Considering the likely effect of slimes on performance, the 53 μm grind size is preferable. A reasonable upgrade of HREO can be achieved (Fig. 18A), but if targeting all REE-bearing minerals, LREO are not effectively recovered.

The general trends of these charts follow a similar pattern to those shown in Fig. 16. In Fig. 18B, generally expected grade-recovery trends are observed, this is because all minerals are targeted. Where there are deviations this is a result of unliberated particles and recovery of particles with low HREO grade. For Fig. 18A, the same issues apply but are compounded by targeting of apatite which has relatively low LREO content compared to synchysite-(Ce). Synchysite-(Ce) is also targeted but as there are larger abundances of apatite in the sample there is a complicated trend.

Comparing Figs. 16 and 18, sequential separation would represent a reasonable processing route to maximise processing efficiency.

5.6. Leaching

Mineralogy, liberation and mineral association are the most important parameters to be taken into account when assessing the leachability of the ore under investigation. A chemical treatment can be applied either to the whole rock or to a specific ore concentrate, obtained by physical beneficiation. It can also be applied to specific size fractions, for example the very fine particles of < 20 μm that form about 50% of the ore deposit which may consider difficult to be processed using physical processing methods.

The major gangue minerals at Songwe Hill are ankerite and calcite, respectively comprising about 30% and 27% of the ore deposit. Thus, acid leaching could be an appropriate process to reduce the major gangue minerals but such a process would result in excessive acid consumption. Regeneration of HCl from a leach solution has been developed for treating REE-bearing carbonate and apatite minerals (Girgin et al., 2013). This is undertaken by reacting $CaCl_2$ from the gangue leach solution with concentrated H_2SO_4 to generate HCl and insoluble calcium sulphate phases $CaSO_4{\cdot}xH_2O$ such as gypsum, hemihydrate and anhydrite. These products can be separated out from the liquid by filtration (Demopoulos et al., 2008; Al-Othman and Demopoulos, 2009). However, sulphuric acid is not an efficient acid to process deposits containing phosphate minerals as the acid will react with phosphate minerals (e.g. apatite) generating “phosphogypsum”. Phosphogypsum can incorporate notable concentrations of rare earth elements from solution, and the generation of phosphogypsum can be considered as an environmental issue due to the presence of toxic metals and radionuclides (Rutherford et al., 1994; Samonov, 2011;

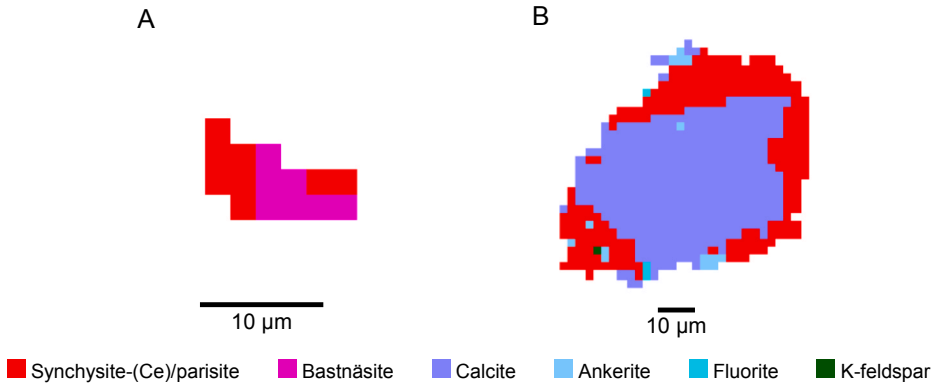

Fig. 17. Examples of particles which result in deviations from expected grade-recovery behaviour. (A) particle containing significant proportion of bastnäsite which has relatively low LREO content. (B) Unliberated particle with higher grade of synchysite-(Ce) at surface (63.5% vol.) than in the overall particle (35.5% vol.). False colour mineral map images generated by QEMSCAN®.

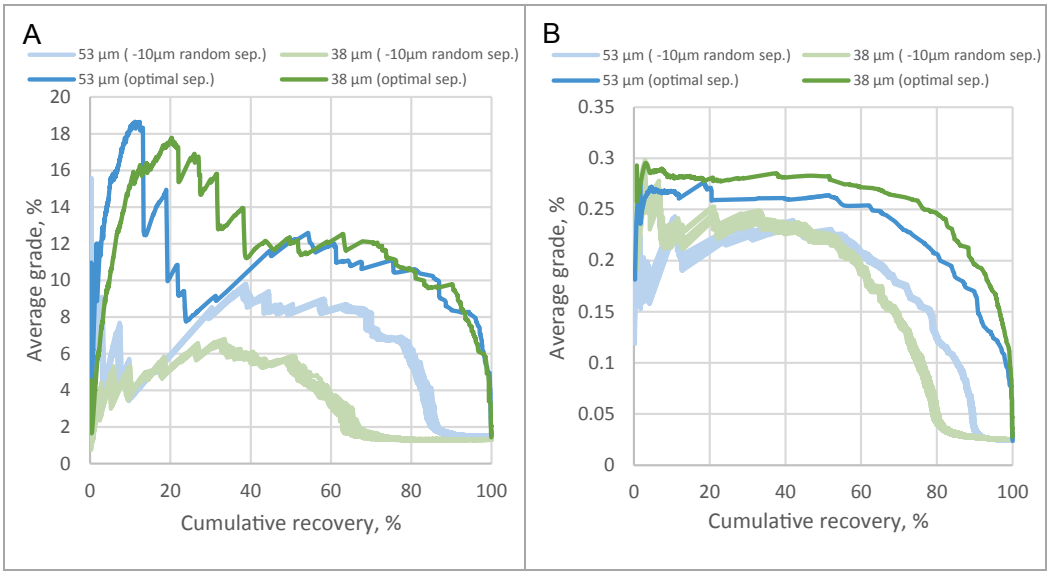

Fig. 18. Theoretical grade recovery curves of (A) LREO and (B) HREO for grind sizes of P_{80} 53 µm and P_{80} 38 µm based on data generated by QEMSCAN®. Curves created based on fraction of REE-bearing minerals exposed on the surface. Darker lines represent perfect separation from high to low surface exposure. Lighter lines represent a simulation of the effects of slimes on flotation with random recovery of −10 µm particles. Ten random simulations were undertaken to evaluate the range of TGR.

Peelman et al., 2014; Valkov et al., 2014).

6. A potential beneficiation flowsheet

In order to separate REE-bearing minerals form their gangue matrices at Songwe Hill the following flowsheet may be a potential processing option. The first step comprises crushing and grinding the composite sample to P_{80} of 53 µm, followed by magnetic separation and froth flotation (Fig. 19). Grinding the composite sample to P_{80} of 53 µm will increase the liberation of the valuable minerals. Further grinding to P_{80} of 38 µm will lead to highly improved liberation of the valuable minerals, at the expense of generating further fines. Adding a pre-concentration step using magnetic separation prior to flotation process reduces the percentage of magnetic gangue minerals e.g. ankerite and iron oxides/carbonates, which comprise ~50 wt% of the gangue. This minimizes chemical reagent consumption for the flotation process and acid consumption of the gangue leach of the rougher concentrate.

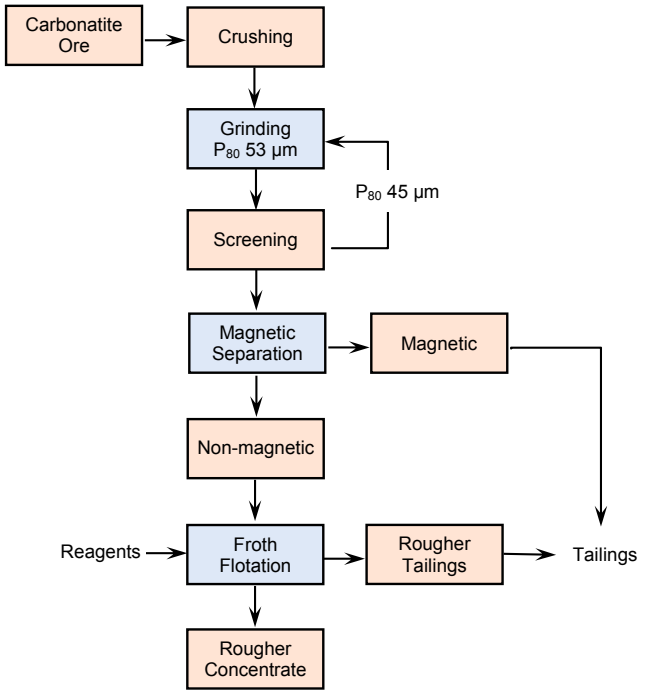

Fig. 19. A potential metallurgical beneficiation flowsheet to process the Songwe Hill deposit.

7. Conclusions

- At the Songwe Hill carbonatite deposit, apatite hosts HREE including 50% of Gd, 63% of Dy and 71% of Y, while synchysite-(Ce) with much less common syntaxially intergrown parisite-(Ce), mainly hosts LREE (including Nd) and the remaining Gd, Dy and Y, whereas the less common florencite-(Ce), accommodates the rest of LREE. Although the ore mineralogy is complex, it is consistent throughout the deposit so that one metallurgical approach may be applied.
- Successful separation of REE ore deposits not only depends on the differences in the physical and chemical properties between the valuable and gangue minerals, but also on the detailed determination of mineralogical parameters such as mineral chemistry, liberation, association and grain size distribution. For example, the main REE fluorcarbonates, bastnäsite, parisite and synchysite have very different magnetic properties, and each mineral has further discrete species depending on the predominant REE, for example, synchysite-(Ce), synchysite-(Y), and synchysite-(Nd). All of these species will vary in their properties in terms of magnetism and density and each species needs a different way to be separated.
- The quantitative mineralogical data based on the mass distribution of REE-bearing minerals within size-density classes indicates that gravity separation would be unlikely to be an effective means of processing the ore to upgrade REE-bearing minerals due to the narrow density difference between REE-bearing minerals and the overall sample. A potential pre-concentrate of the > 500 µm size fraction could be achieved using dense medium separation, but with a limited level of upgrade.
- The quantitative mineralogical data based on the surface area of exposed REE-bearing minerals reveals that targeting both apatite and synchysite-(Ce) instead of only synchysite-(Ce) using flotation technique would be a reasonable processing route to recover LREO and HREO and maximise processing efficiency as indicated from the

TGR curves.

- Synchysite-(Ce), at Songwe Hill, is strongly associated with other gangue minerals and separation would involve fine grinding. The deposit consists of a considerable amount (~43 wt%) of paramagnetic gangue minerals including ankerite and iron oxides/carbonates which could be removed using magnetic separation. Apatite and synchysite-(Ce) could be separated using froth flotation as they have similar surface properties towards the same collectors such as fatty acids. Thus, a potential processing flowsheet would apply a combination of fine grinding along with magnetic separation and froth flotation.

CRediT authorship contribution statement

Safaa Al-Ali: Conceptualization, Investigation, Writing - original draft, Writing - review & editing, Visualization, Funding acquisition. **Frances Wall:** Conceptualization, Supervision, Writing - review & editing, Funding acquisition. **Robert Fitzpatrick:** Software, Formal analysis, Investigation, Data curation, Visualization, Writing - review & editing. **Sam Broom-Fendley:** Conceptualization, Validation, Investigation, Writing - review & editing. **Gavyn Rollinson:** Formal analysis, Investigation, Data curation. **Aoife E. Brady:** Formal analysis, Investigation. **Jonathan R. Pickles:** Formal analysis. **Adam Williams:** Investigation. **Will Dawes:** Resources, Supervision, Project administration.

Declaration of Competing Interest

The authors declare that they have no known competing financial interests or personal relationships that could have appeared to influence the work reported in this paper.

Acknowledgments

The authors would like to thank Mkango Resources Ltd including Dr. Paul Armitage for provision of drill core samples and corresponding data for the Songwe Hill carbonatite deposit, Malawi. This study was funded by the Higher Committee of Education Development in Iraq (HCED) scholarship to Safaa Al-Ali (D-09-3573) and part-funded by the Natural Environment Research Council (NERC) SoS RARE (NE/M011429/1), EU H2020 HiTechAlkCarb (grant agreement no. 689909) and NERC Industrial Innovation Fellowship (NE/R013403/1) projects. The research data supporting this publication are openly available from the University of Exeter's institutional repository at http://hdl.handle.net/10871/28823.

References

Al-Ali, S., Wall, F., Sheridan, R., Pickles, J., Pascoe, R., 2019. Magnetic properties of REE fluorcarbonate minerals and their implications for minerals processing. Miner. Eng. 131, 392–397.

Al-Othman, A., Demopoulos, G.P., 2009. Gypsum crystallization and hydrochloric acid regeneration by reaction of calcium chloride solution with sulfuric acid. Hydrometallurgy 96, 95–102.

Avalon Rare Metals Inc., 2013. Technical Report disclosing the results of the feasibility study on the Nechalacho Rare Earth Elements Project. Technical Report (NI 43-101) – English, 291 pp. www.sedar.com, accessed 25.4.20.

Broom-Fendley, S., Brady, A.E., Horstwood, M.S.A., Wooley, A.R., Mtegha, J., Wall, F., Dawes, W., Gunn, G., 2017a. Geology, geochemistry and geochronology of the Songwe Hill carbonatite, Malawi. J. Afr. Earth Sc. 134, 10–23.

Broom-Fendley, S., Brady, A.E., Wall, F., Gunn, G., Dawes, W., 2017b. REE minerals at the Songwe Hill carbonatite, Malawi: HREE-enrichment in late-stage apatite. Ore Geol. Rev. 81, 23–41.

Broom-Fendley, S., Styles, M.T., Appleton, J.D., Gunn, G., Wall, F., 2016. Evidence for dissolution-reprecipitation of apatite and preferential LREE mobility in carbonatite-derived late-stage hydrothermal processes. Am. Mineral. 101, 596–611.

Bulatovic, S.M., 2010. Handbook of Flotation Reagents: Chemistry, Theory and Practice - Flotation of Gold, PGM and Oxide Minerals. Elsevier Science.

Burmaa, G., Temuujin, J., Welham, N.J., 2007. Effect of pretreatment on synchysite-Ce ($CaCe(CO_3)_2F$) leaching. Miner. Eng. 20 (8), 807–809.

Chakhmouradian, A.R., Wall, F., 2012. Rare earth elements: Minerals, mines, magnets (and more). Elements 8 (5), 333–340.

Dahlberg, P.S., Noble, A., Pickarts, J.T., Rose, W.L., Jaacks, J., 2014. Bear Lodge project Canadian NI 43-101 pre-feasibility study report on the reserves and development of the Bull Hill Mine, Wyoming. Rare element resources release, 516 p.

Daigle, P., 2012. Rare Earth Metals Inc.: Technical report on the resources estimation of the Lavergne-Springer REE project, Ontario, Canada. NI 43-101 report. Tetra Tech Wardrop.

Demopoulos, G.P., Li, Z., Becze, L., Moldoveanu, G., Cheng, T.C., Harris, B., 2008. New technologies for HCl regeneration in chloride hydrometallurgy. World Metall.-Erzmetall 61, 89–98.

Deng, T., Hill, G., 2014. Flotation of REE bearing minerals from silicate and carbonate host deposits In: Proceeding of the 53rd Annual Conference of Metallurgists. The Canadian Institute of Mining, Metallurgy and Petroleum.

Dho, H., Iwasaki, I., 1990. Role of sodium silicate in phosphate flotation. Miner. Metall. Process. 7 (4), 215–221.

Evans, C.L., Wightman, E.M., Manlapig, E.V., Coulter, B.L., 2011. Application of process mineralogy as a tool in sustainable processing. Miner. Eng. 24 (12), 1242–1248.

Falconer, A., 2003. Gravity separation: old technique/new methods. Phys. Separat. Sci. Eng. 12 (1), 31–48.

Fuerstenau, D.W., Pradip, Herrera-Urbina, R., 1992. The surface chemistry of bastnaesite, barite and calcite in aqueous carbonate solutions. Colloids Surfaces, 68(1–2), 95–102.

Fuerstenau, D.W., Pradip, Khan, L.A., Raghavan, S., 1982. An alternative reagent scheme for the flotation of Mountain Pass rare-earth ore. In: Proceedings of the XIV International Mineral Processing Congress. The Canadian Institute of Mining, Metallurgy and Petroleum, pp. 1–12.

Girgin, S., Feldmann, T., Humphrey, S., Demopoulos, GP., 2013. Low temperature (T < 100C) regeneration of HCl from chloride leaching of Ca-bearing minerals. Conference of Metallurgists. Montreal, Quebec, Canada.

Gottlieb, P., Wilkie, G., Sutherland, D., Ho-Tun, E., Suthers, S., Perera, K., Jenkins, B., Spencer, S., Butcher, A., Rayner, J., 2000. Using quantitative electron microscopy for process mineralogy applications. JOM 52 (4), 24–25.

Grammatikopoulos, T., Mercer, W., Gunning, C., 2013. Mineralogical characterisation using QEMSCAN of the Nechalacho heavy rare earth metal deposit, Northwest Territories, Canada. Can. Metall. Q. 52 (3), 265–277.

Guimarães, R.C., Araujo, A.C., Peres, A.E.C., 2005. Reagents in igneous phosphate ores flotation. Miner. Eng. 18 (2), 199–204.

Gupta, A., Yan, D., 2016. Mineral Processing Design and Operation: An Introduction. Elsevier B.V.

Haumdas, A., Burmaa, G., Bayar, G., Myagmarjav, B., Rakaev, B., 1995. Synchysite – new resources of the rare earths In: Proceedings of the 3rd International Conference on Rare Earth Development and Applications. Baotou, Metallurgical Industry Press, pp. 718–727.

Hogarth, D.D., Hartree, R., Loop, J., Solberg, T.N., 1985. Rare-earth element minerals in four carbonatites near Gatineau, Quebec. Am. Mineral. 70 (11–12), 1135–1142.

Hyland, S., Ulrich, S., 2014. Technical report on the Kyzyl ompul licence, Kyrgyz Republic for Powertech Uranium Corp., Azarga Resources Limited, and UrAsia in Kyrgyzstan LLC. NI 43-101 report. Ravensgate.

Jackson, W.D., Christiansen, G., 1993. International strategic minerals inventory summary report - Rare earth oxides. Circular 930-N. USGS.

Jiao, Y., Qui, K.-H., Zhang, P.-C., Li, J.-F., Zhang, W.-T., Chen, X.-F., 2020. Process mineralogy of Dalucao rare earth ore and design of beneficiation process based on AMICS. Rare Met. 39, 959–966.

Jordens, A., Cheng, Y.P., Waters, K.E., 2013. A review of the beneficiation of rare earth element bearing minerals. Miner. Eng. 41, 97–114.

Jordens, A., Marion, C., Grammatikopoulos, T., Hart, B., Waters, K.E., 2016. Beneficiation of the Nechalacho rare earth deposit: Flotation response using benzohydroxamic acid. Miner. Eng. 99, 158–169.

Kawatra, S.K., Carlson, J.T., 2014. Beneficiation of phosphate ore. Society for Mining, Metallurgy and Exploration.

Kelly, E.G., Spottiswood, D.J., 1982. Introduction to Mineral Processing. Wiley, New York.

Klimpel, R.R. 1998. Introduction to solid-solid separation of fine particles by froth flotation. NSF Engineering Resource Centre for Particle Science and Technology, University of Florida.

Krishnamurthy, N., Gupta, C.K., 2016. Extractive Metallurgy of Rare Earths. CRC Press.

Kynicky, J., Smith, M.P., Xu, C., 2012. Diversity of rare earth deposits: The key example of China. Elements 8 (5), 361–367.

Leal Filho, L.S., Seidl, P.R., Correia, J.C.G., Cerqueira, L.C.K., 2000. Molecular modelling of reagents for flotation processes. Miner. Eng. 13 (14–15), 1495–1503.

Lotter, N.O., Whittaker, P.J., Kormos, L., Stickling, J.S., Wilkie, G.J., 2002. The development of process mineralogy at Falconbridge Limited, and application to the Raglan mill. CIM Bull. 95 (1066), 85–92.

Mariano, A.N., Mariano, A., 2012. Rare earth mining and exploration in North America. Elements 8 (5), 369–376.

Martienssen, W., 2005. The elements. In: Martienssen, W., Warlimont, H. (Eds.), Springer Handbook of Condensed Matter and Materials Data. Springer, Berlin Heidelberg, pp. 45–158.

McIvor, R.E., Finch, J.A., 1991. A guide to interfacing of plant grinding and flotation operations. Miner. Eng. 4 (1), 9–23.

Nivin, V.A., Treloar, P.J., Konopleva, N.G., Ikorsky, S.V., 2005. A review of the occurrence, form and origin of C-bearing species in the Khibiny Alkaline Igneous Complex, Kola Peninsula. NW Russia. Lithos 85 (1–4), 93–112.

Owens, C.L., Nash, G.R., Hadler, K., Fitzpatrick, R.S., Anderson, C.G., Wall, F., 2018. Zeta potentials of the rare earth element fluorcarbonate minerals focusing on bastnäsite and parisite. Adv. Colloid Interface Sci. 256, 152–162.

Owens, C.L., Schach, E., Heinig, T., Rudolph, M., Nash, G.R., 2019. Surface nanobubbles

on the rare earth fluorcarbonate mineral synchysite. J. Colloid Interface Sci. 552, 66–71.
Pascoe, R.D., Power, M.R., Simpson, B., 2007. QEMSCAN analysis as a tool for improved understanding of gravity separator performance. Miner. Eng. 20 (5), 487–495.
Peak Resources Ltd. Ngualla Rare Earth Project. Available online: https://www.peakresources.com.au/tanzania (accessed on 21 July 2019).
Peelman, S., Sun, Z.H., Sietsma, J., Yang, Y., 2014. Leaching of rare earth elements: Past and present. ERES2014: First European rare earth resources conference. Milos, Greece.
Pradip, Fuerstenau, D.W., 1991. The role of inorganic and organic reagents in the flotation separation of rare-earth ores. Int. J. Mineral Process., 32(1–2), 1–22.
Pradip, Fuerstenau, D.W., 2013. Design and development of novel flotation reagents for the beneficiation of Mountain Pass rare-earth ore. Min. Metall. Process. 30(1), 1–9.
Rollinson, G.K., Andersen, J.C.Ø., Stickland, R.J., Boni, M., Fairhurst, R., 2011. Characterisation of non-sulphide zinc deposits using QEMSCAN®. Miner. Eng. 24 (8), 778–787.
Ruberti, E., Enrich, G.E.R., Gomes, C.B., Comin-Chiaramonti, P., 2008. Hydrothermal REE fluorocarbonate mineralization at Barra do Itapirapua, a multiple stockwork carbonate, southern Brazil. Can. Mineralog. 46 (4), 901–914.
Rutherford, P.M., Dudas, M.J., Samek, R.A., 1994. Environmental impacts of phosphogypsum. Sci. Total Environ. 149 (1–2), 1–38.
Samonov, A.E., 2011. New data on mineral forms of rare metals in phosphogypsum wastes. Dokl. Earth Sci. 440 (1), 1312–1315.
Santana, R.C., Farnese, A.C., Fortes, M.C., Ataíde, C.H., Barrozo, M.A., 2008. Influence of particle size and reagent dosage on the performance of apatite flotation. Sep. Purif. Technol. 64 (1), 8–15.
Stans Energy Corp. Overview of historical REM reserves in Kutessay II from Kyrgyz. Available online: http://www.stansenergy.com/K_Overview.htm (accessed on 08 December 2019).
Schulz, B., Merker, G., Gutzmer, J., 2019. Automated SEM mineral liberation analysis (MLA) with generically labelled EDX spectra in the mineral processing of rare earth element ores. Minerals 9 (9), 527.
Sindern, S., Meyer, F.M., 2016. Automated quantitative rare earth elements mineralogy by scanning electron microscopy. Phys. Sci. Rev. 1 (9).
Tickell, F.G., 2011. The Techniques of Sedimentary Mineralogy, vol. 4 Elsevier.
Valkov, A.V., Andreev, V.A., Anufrieva, A.V., Makaseev, Y.N., Bezrukova, S.A., Demyanenko, N.V., 2014. Phosphogypsum technology with the extraction of valuable components. Procedia Chem. 11, 176–181.
Van Rythoven, A.D., Pfaff, K., Clark, J.G., 2020. Use of QEMSCAN® to characterize oxidized REE ore from the Bear Lodge carbonatite, Wyoming, USA. Ore Energy Resource Geol. 2–3, 100005.
Verplanck, P.L., Farmer, G.L., Mariano, A.N., 2015. Nd and Sr isotopic composition of rare earth element mineralized carbonatites In: Simandl, G.J., Neetz, M. (Eds.), Symposium on Strategic and Critical Materials Proceedings. British Columbia Ministry of Energy and 230 Mines, British Columbia Geological Survey, pp. 65–68.
Wall, F., 2014. Rare earth elements. In: Gunn, G. (Ed.), Critical Metals Handbook. John Wiley & Sons, pp. 312–339.
Wall, F., Mariano, A., 1996. Rare earth minerals in carbonatites: A discussion centred on the Kangankunde Carbonatite, Malawi. In: Jones, A., Wall, F., Williams, C.T. (Eds.), Rare Earth Minerals: Chemistry, Origin and ore Deposits. Volume 6 of Minerlaogical Society Series. Chapman and Hall, pp. 193–225.
Wang, L., Ni, Y., Hughes, J.M., Bayliss, P., Drexler, J.W., 1994. The atomic arrangement of synchysite-(Ce), $CeCaF(CO_3)_2$. Can. Mineralog. 32, 865–871.
Williams, A., 2019. Correlating mineralogy with downhole magnetic susceptibility and conductivity in relation to rare earth carbonatite mineralisation at Songwe Hill, Malawi. Master dissertation. University of Exeter.
Wills, B.A., Finch, J.A., 2016. Wills' Mineral Processing Technology. Elsevier Ltd.
Witley, C., Swinden, S., Trusler, G., Dempers, N., 2020. Mkango Resources Limited: Songwe Hill rare earth element (REE) project Phalombe district, Republic of Malawi. NI 43-101 TECHNICAL report. MSA Group (Pty) Ltd.
Woolley, A.R., Kempe, D.R.C., 1989. Carbonatites-nomenclature, average chemical compositions, and element distribution. In: Bell, K. (Ed.), Carbonatites—Genesis and Evolution. Unwin Hyman, London, pp. 1–14.
Yu, B., Aghamirian, M., 2015. REO mineral separation from silicates and carbonate gangue minerals. Can. Metall. Q. 54 (4), 377–387.